Journal of Cosmology and Astroparticle Physics
An IOP and SISSA journal

# On the validity of the effective field theory for dark matter searches at the LHC, part II: complete analysis for the $s$-channel

**Giorgio Busoni,**[a] **Andrea De Simone,**[a] **Johanna Gramling,**[b] **Enrico Morgante**[b] **and Antonio Riotto**[b]

[a]SISSA and INFN, Sezione di Trieste,
Via Bonomea 265, I-34136 Trieste, Italy
[b]Section de Physique, Université de Genève,
24 quai E. Ansermet, CH-1211 Geneva, Switzerland

E-mail: giorgio.busoni@sissa.it, andrea.desimone@sissa.it, johanna.gramling@unige.ch, enrico.morgante@unige.ch, antonio.riotto@unige.ch

Received February 25, 2014
Accepted May 30, 2014
Published June 27, 2014

**Abstract.** We generalize in several directions our recent analysis of the limitations to the use of the effective field theory approach to study dark matter at the LHC. Firstly, we study the full list of operators connecting fermion DM to quarks and gluons, corresponding to integrating out a heavy mediator in the $s$-channel; secondly, we provide analytical results for the validity of the EFT description for both $\sqrt{s} = 8$ TeV and 14 TeV; thirdly, we make use of a MonteCarlo event generator approach to assess the validity of our analytical conclusions. We apply our results to revisit the current collider bounds on the ultraviolet cut-off scale of the effective field theory and show that these bounds are weakened once the validity conditions of the effective field theory are imposed.

**Keywords:** dark matter theory, dark matter experiments

**ArXiv ePrint:** 1402.1275



doi:10.1088/1475-7516/2014/06/060

JCAP06(2014)060

## Contents


**1 Introduction** **1**

**2 Validity of the EFT: analytical approach** **3**
2.1 Operators and cross sections 3
2.2 Results and discussion 6

**3 Comparison with MonteCarlo simulations** **7**
3.1 Simulation and analysis description 10
3.2 Results 10

**4 Implications of the limited validity of EFT in DM searches at LHC** **12**

**5 Conclusions** **14**

**A Three-body cross sections** **15**
A.1 Generalities 15
A.2 Matrix elements 16
A.3 Cross sections 20


## 1 Introduction

While there are many cosmological and astrophysical evidences that our universe contains a sizable amount of dark Matter (DM), i.e. a component which clusters at small scales, its nature is still a mystery. Various considerations point towards the possibility that DM is made of neutral particles whose mass and interactions are dictated by physics in the electroweak energy range. If so, the DM relic density of these particles, assuming they were in thermal equilibrium during the evolution of the universe, turns out to be

$$\left(\frac{\Omega_{\rm DM}h^2}{0.110}\right) \approx \frac{3\times 10^{-26}{\rm cm}^3/{\rm sec}}{\langle\sigma v\rangle_{\rm ann}}, \tag{1.1}$$

where $\langle\sigma v\rangle_{\rm ann}$ is the (thermally-averaged) annihilation cross section. A weak interaction strength provides the abundance in the right range measured by the Planck collaboration: $\Omega_{\rm DM} = 0.315 \pm 0.0175$ [1]. This numerical coincidence represents the main reason why it is generically believed that DM is made of weakly-interacting particles with a mass in the range $(10^2 - 10^4)$ GeV.

Currently, there are several ways to search for such DM candidates. Apart from the indirect [2] and direct [3] searches, DM particles (if they are light enough) might reveal themselves in particle colliders, namely at the LHC. Many LHC searches for DM are based on the idea of looking at events with missing energy plus a single jet or photon, emitted from the initial state in $pp$ collisions (for alternative kinds of DM searches at the LHC see e.g. refs. [4–9])

$$pp \to \chi + \overline{\chi} + \text{jet/photon}, \tag{1.2}$$

where $\chi$ indicates the DM particle. Several results are already available from two LHC collaborations [10–17].



JCAP06(2014)060

In order to avoid the overwhelming model-dependence introduced by the plethora of DM models discussed in the literature, DM searches at the LHC have made use of the Effective Field Theory (EFT) [18–28]. This approach is a very powerful and economical way to grasp the main features of a physical process, only in terms of the degrees of freedom which are excited at the scale of the process. EFT techniques are successfully applied in many branches of physics, and in particular they have become a standard way to present experimental results for DM searches.

However, as far as collider searches are concerned, with the LHC being such a powerful machine, it is not guaranteed that the events used to constrain an effective interaction are not occurring at an energy scale larger than the cutoff scale of the effective description. In other words, some (or many) events of DM production may occur with such a high momentum transfer that the EFT is not a good description anymore. The question about the validity of the EFT for collider searches of DM has become pressing (see also refs. [7, 21, 29–35]), especially in the perspective of analysing the data from the future LHC run at (13-14) TeV.

Let us consider a simple model where there is a heavy mediator of mass $M$, to which the quarks and DM are coupled with couplings $g_q$ and $g_\chi$, respectively. The EFT is a good approximation only at low energies. Indeed, it is possible at low energies to integrate out the heavy mediator from the theory and obtain a tower of operators. The matching condition of the ultra-violet (UV) theory with the mediator and its low-energy effective counterpart implies $\Lambda = M/\sqrt{g_q g_\chi}$. A DM production event occurs at an energy at which the EFT is reliable as long as $Q_{\rm tr} < M$, where $Q_{\rm tr}$ is the momentum transfer in the process; this, together with the condition of perturbativity of the couplings $g_{q,\chi} < 4\pi$, implies

$$\Lambda > \frac{Q_{\rm tr}}{\sqrt{g_q g_\chi}} > \frac{Q_{\rm tr}}{4\pi}\,. \tag{1.3}$$

If, in addition, one assumes the momentum transfer to occur in the $s$-channel, then kinematics imposes $Q_{\rm tr} > 2m_{\rm DM}$, so eq. (1.3) becomes

$$\Lambda > \frac{m_{\rm DM}}{2\pi}\,. \tag{1.4}$$

This is a very minimal requirement which is refined event-by-event by the stronger condition eq. (1.3), which depends on $m_{\rm DM}$ through $Q_{\rm tr}$. It is clear that the details of condition (1.3) depend on the values of the couplings in the UV theory. In the following, for definiteness, we will mostly identify the mass of the new degrees of freedom $M$ with the suppression scale of the operator $\Lambda$. This is equivalent to consider couplings in the UV theory of $\mathcal{O}(1)$. So, we will deal with the condition (but we will discuss also the impact of taking couplings larger than 1)

$$Q_{\rm tr} \lesssim \Lambda\,. \tag{1.5}$$

In ref. [29] we have started the discussion of the limitations to the use of the EFT approach for DM searches at the LHC by adopting a toy model where the heavy mediator is exchanged in the $s$-channel and by introducing a few quantities which quantify the error made when using effective operators to describe processes with very high momentum transfer. Our criteria indicated up to what cutoff energy scale, and with what precision, the effective description is valid, depending on the DM mass and couplings. In this paper we significantly extend our previous work along four different directions:

1. we consider the full list of operators connecting fermion DM to quarks and corresponding to integrating out the heavy mediator in the $s$-channel;



JCAP06(2014)060

2. we provide analytical results for the validity of the EFT description for both $\sqrt{s} = 8$ TeV and 14 TeV;

3. we follow a MonteCarlo approach to assess the validity of the EFT and compare this fully numerical results with the analytical calculations;

4. we apply our results to revisit the current experimental bounds on the effective operator scale; by requiring that only the events which are "safe" from the EFT point of view should be considered, the bounds get weakened.

The rest of the present paper is organized as follows. In section 2 we present and discuss the results of our analytical approach to assess the validity of EFT. In section 3, the fully numerical approach is described and the results are compared with the analytical calculations. In section 4 we analyze the impact of the limitation of the validity of the EFT for the current limits from the LHC searches. Finally, we draw our conclusions in section 5. The details of the analytical results can be found in the appendix A.

## 2 Validity of the EFT: analytical approach

### 2.1 Operators and cross sections

The starting point of our analysis is the list of the 18 operators reported in table 1 which are commonly used in the literature [18]. We have considered not only the operators connecting the DM fermion to quarks (D1-D10), but also those involving gluon field strengths (D11-D14). Furthermore, the operators can originate from heavy mediators exchange in the $s$-channel. For instance, the D1' (D5) operators may be originated by the tree-level $s$-channel exchange of a very heavy scalar (vector) boson $S$ ($V_\mu$), with lagrangians

$$\mathscr{L}_{\mathrm{D1'}} \supset \frac{1}{2} M^2 S^2 - g_q \bar{q} q S - g_\chi \bar{\chi} \chi S \,, \tag{2.1}$$

$$\mathscr{L}_{\mathrm{D5}} \supset \frac{1}{2} M^2 V^\mu V_\mu - g_q \bar{q} \gamma^\mu q V_\mu - g_\chi \bar{\chi} \gamma^\mu \chi V_\mu \,. \tag{2.2}$$

Notice the presence of the "primed" operators $D1'$–$D4'$, very similar to the ones often considered $D1$–$D4$, respectively, but with a different normalization, independent of the quark masses. In fact, they may arise from integrating out heavy scalars which do not take a vacuum expectation value and therefore do not give rise to quark masses.[1]

We have computed the tree-level differential cross sections in the transverse momentum $p_{\mathrm{T}}$ and rapidity $\eta$ of the final jet for the hard scattering process with gluon radiation from the initial state $f(p_1) + \bar{f}(p_2) \to \chi(p_3) + \chi(p_4) + g(k)$, where $f$ is either a quark (for operators

[1] A normalization proportional to the quark mass is common in many models motivated by flavour physics, but in general the coefficient $\Lambda^3$ at the denominator can have a different form. For example, if the effective operators come from a Naturalness-motivated new physics theory like Supersymmetry or Composite Higgs Models, assuming a $\mathrm{U}(2)^3$ flavour symmetry [36, 37] the normalization would be

$$\lambda_{t,b} \frac{1}{\Lambda^2} \frac{m_q}{m_{t,b}} \tag{2.3}$$

where $\Lambda$ is an energy scale of the order some TeV related to the Electroweak Symmetry Breaking and $m_{t,b}, \lambda_{t,b}$ are the mass and the Yukawa coupling with the Higgs of the top/bottom quark, depending on whether the quark $q$ is up-like or down-like. In the present work, we will be agnostic about this point, and we'll keep both the primed and unprimed operators into account on the same footing as all others.



JCAP06(2014)060

| Name | Operator | Coefficient |
|---|---|---|
| D1 | $\bar{\chi}\chi\ \bar{q}q$ | $m_q/\Lambda^3$ |
| D1' | $\bar{\chi}\chi\ \bar{q}q$ | $1/\Lambda^2$ |
| D2 | $\bar{\chi}\gamma^5\chi\ \bar{q}q$ | $im_q/\Lambda^3$ |
| D2' | $\bar{\chi}\gamma^5\chi\ \bar{q}q$ | $i/\Lambda^2$ |
| D3 | $\bar{\chi}\chi\ \bar{q}\gamma^5 q$ | $im_q/\Lambda^3$ |
| D3' | $\bar{\chi}\chi\ \bar{q}\gamma^5 q$ | $i/\Lambda^2$ |
| D4 | $\bar{\chi}\gamma^5\chi\ \bar{q}\gamma^5 q$ | $m_q/\Lambda^3$ |
| D4' | $\bar{\chi}\gamma^5\chi\ \bar{q}\gamma^5 q$ | $1/\Lambda^2$ |
| D5 | $\bar{\chi}\gamma_\mu\chi\ \bar{q}\gamma^\mu q$ | $1/\Lambda^2$ |
| D6 | $\bar{\chi}\gamma_\mu\gamma^5\chi\ \bar{q}\gamma^\mu q$ | $1/\Lambda^2$ |
| D7 | $\bar{\chi}\gamma_\mu\chi\ \bar{q}\gamma^\mu\gamma^5 q$ | $1/\Lambda^2$ |
| D8 | $\bar{\chi}\gamma_\mu\gamma^5\chi\ \bar{q}\gamma^\mu\gamma^5 q$ | $1/\Lambda^2$ |
| D9 | $\bar{\chi}\sigma_{\mu\nu}\chi\ \bar{q}\sigma^{\mu\nu} q$ | $1/\Lambda^2$ |
| D10 | $\bar{\chi}\sigma_{\mu\nu}\gamma^5\chi\ \bar{q}\sigma^{\mu\nu} q$ | $i/\Lambda^2$ |
| D11 | $\bar{\chi}\chi\ G^{\mu\nu}G_{\mu\nu}$ | $\alpha_s/4\Lambda^3$ |
| D12 | $\bar{\chi}\gamma^5\chi\ G^{\mu\nu}G_{\mu\nu}$ | $i\alpha_s/4\Lambda^3$ |
| D13 | $\bar{\chi}\chi\ G^{\mu\nu}\tilde{G}_{\mu\nu}$ | $i\alpha_s/4\Lambda^3$ |
| D14 | $\bar{\chi}\gamma^5\chi\ G^{\mu\nu}\tilde{G}_{\mu\nu}$ | $\alpha_s/4\Lambda^3$ |

**Table 1**. Operators used throughout this work. The nomenclature is mostly taken from ref. [21].

D1-D10), or a gluon (for operators D11-D14). The results are conveniently written in terms of the momentum transfer in the $s$-channel

$$Q_{\rm tr}^2 = (p_1 + p_2 - k)^2 = x_1 x_2 s - \sqrt{s}\, p_{\rm T} \left(x_1 e^{-\eta} + x_2 e^{\eta}\right) , \tag{2.4}$$

where $x_1, x_2$ are the fractions of momentum carried by initial partons and $\eta, p_{\rm T}$ are the pseudo-rapidity and the transverse momentum of the final state gluon, respectively. The expressions are of course valid for all admitted values of the parameters. It's only when integrated numerically over the PDFs and over $\eta, p_{\rm T}$ that the dependence on these values comes in. We obtain

$$\left.\frac{{\rm d}^2\hat{\sigma}}{{\rm d}p_{\rm T}{\rm d}\eta}\right|_{D1'} = \frac{\alpha_s}{36\pi^2}\frac{1}{p_{\rm T}}\frac{1}{\Lambda^4}\frac{\left[Q_{\rm tr}^2 - 4m_{\rm DM}^2\right]^{3/2}\left[1 + \frac{Q_{\rm tr}^4}{(x_1x_2s)^2}\right]}{Q_{\rm tr}} , \tag{2.5}$$

$$\left.\frac{{\rm d}^2\hat{\sigma}}{{\rm d}p_{\rm T}{\rm d}\eta}\right|_{D4'} = \frac{\alpha_s}{36\pi^2}\frac{1}{p_{\rm T}}\frac{1}{\Lambda^4} Q_{\rm tr}\left[Q_{\rm tr}^2 - 4m_{\rm DM}^2\right]^{1/2}\left[1 + \frac{Q_{\rm tr}^4}{(x_1x_2s)^2}\right] , \tag{2.6}$$

$$\left.\frac{{\rm d}^2\hat{\sigma}}{{\rm d}p_{\rm T}{\rm d}\eta}\right|_{D5} = \frac{\alpha_s}{27\pi^2}\frac{1}{p_{\rm T}}\frac{1}{\Lambda^4}\frac{\left[Q_{\rm tr}^2 - 4m_{\rm DM}^2\right]^{1/2}\left[Q_{\rm tr}^2 + 2m_{\rm DM}^2\right]\left[1 + \frac{Q_{\rm tr}^4}{(x_1x_2s)^2} - 2\frac{p_{\rm T}^2}{x_1x_2s}\right]}{Q_{\rm tr}} , \tag{2.7}$$

$$\left.\frac{{\rm d}^2\hat{\sigma}}{{\rm d}p_{\rm T}{\rm d}\eta}\right|_{D8} = \frac{\alpha_s}{27\pi^2}\frac{1}{p_{\rm T}}\frac{1}{\Lambda^4}\frac{\left[Q_{\rm tr}^2 - 4m_{\rm DM}^2\right]^{3/2}\left[1 + \frac{Q_{\rm tr}^4}{(x_1x_2s)^2} - 2\frac{p_{\rm T}^2}{x_1x_2s}\right]}{Q_{\rm tr}} , \tag{2.8}$$

$$\left.\frac{{\rm d}^2\hat{\sigma}}{{\rm d}p_{\rm T}{\rm d}\eta}\right|_{D9} = \frac{2\alpha_s}{27\pi^2}\frac{1}{p_{\rm T}}\frac{1}{\Lambda^4}\frac{\sqrt{Q_{\rm tr} - 4m_{\rm DM}^2}\left[Q_{\rm tr}^2 + 2m_{\rm DM}^2\right]\left[1 + \frac{Q_{\rm tr}^4}{(x_1x_2s)^2} + 4p_{\rm T}^2\left(\frac{1}{Q_{\rm tr}^2} - \frac{1}{x_1x_2s}\right)\right]}{Q_{\rm tr}} ,$$



JCAP06(2014)060

(2.9)

$$\left.\frac{\mathrm{d}^2\hat{\sigma}}{\mathrm{d}p_{\mathrm{T}}\mathrm{d}\eta}\right|_{D11} = \frac{3\alpha_s^3}{256\pi^2\Lambda^6}\frac{(x_1x_2s)^3}{(Q_{\mathrm{tr}}^2-x_1x_2s)^2}\frac{(Q_{\mathrm{tr}}^2-4m_{\mathrm{DM}}^2)^{3/2}}{p_{\mathrm{T}}Q_{\mathrm{tr}}}\left[1-4\frac{Q_{\mathrm{tr}}^2-p_{\mathrm{T}}^2}{x_1x_2s}+\frac{8Q_{\mathrm{tr}}^4+21p_{\mathrm{T}}^4}{(x_1x_2s)^2}\right.$$
$$-2Q_{\mathrm{tr}}^2\frac{5Q_{\mathrm{tr}}^4+4Q_{\mathrm{tr}}^2p_{\mathrm{T}}^2+5p_{\mathrm{T}}^4}{(x_1x_2s)^3}+Q_{\mathrm{tr}}^4\frac{8Q_{\mathrm{tr}}^4+8Q_{\mathrm{tr}}^2p_{\mathrm{T}}^2+5p_{\mathrm{T}}^4}{(x_1x_2s)^4}-4Q_{\mathrm{tr}}^8\frac{Q_{\mathrm{tr}}^2+p_{\mathrm{T}}^2}{(x_1x_2s)^5}$$
$$\left.+\frac{Q_{\mathrm{tr}}^{12}}{(x_1x_2s)^6}\right], \tag{2.10}$$

$$\left.\frac{\mathrm{d}^2\hat{\sigma}}{\mathrm{d}p_{\mathrm{T}}\mathrm{d}\eta}\right|_{D12} = \frac{3\alpha_s^3}{256\pi^2\Lambda^6}\frac{(x_1x_2s)^3}{(Q_{\mathrm{tr}}^2-x_1x_2s)^2}\frac{Q_{\mathrm{tr}}\sqrt{Q_{\mathrm{tr}}^2-4m_{\mathrm{DM}}^2}}{p_{\mathrm{T}}}\left[1-4\frac{Q_{\mathrm{tr}}^2-p_{\mathrm{T}}^2}{x_1x_2s}+\frac{8Q_{\mathrm{tr}}^4+21p_{\mathrm{T}}^4}{(x_1x_2s)^2}\right.$$
$$-2Q_{\mathrm{tr}}^2\frac{5Q_{\mathrm{tr}}^4+4Q_{\mathrm{tr}}^2p_{\mathrm{T}}^2+5p_{\mathrm{T}}^4}{(x_1x_2s)^3}+Q_{\mathrm{tr}}^4\frac{8Q_{\mathrm{tr}}^4+8Q_{\mathrm{tr}}^2p_{\mathrm{T}}^2+5p_{\mathrm{T}}^4}{(x_1x_2s)^4}-4Q_{\mathrm{tr}}^8\frac{Q_{\mathrm{tr}}^2+p_{\mathrm{T}}^2}{(x_1x_2s)^5}$$
$$\left.+\frac{Q_{\mathrm{tr}}^{12}}{(x_1x_2s)^6}\right], \tag{2.11}$$

$$\left.\frac{\mathrm{d}^2\hat{\sigma}}{\mathrm{d}p_{\mathrm{T}}\mathrm{d}\eta}\right|_{D13} = \frac{3\alpha_s^3}{256\pi^2\Lambda^6}\frac{(x_1x_2s)^3}{(Q_{\mathrm{tr}}^2-x_1x_2s)^2}\frac{(Q_{\mathrm{tr}}^2-4m_{\mathrm{DM}}^2)^{3/2}}{p_{\mathrm{T}}Q_{\mathrm{tr}}}\left[1-4\frac{Q_{\mathrm{tr}}^2}{x_1x_2s}+\frac{8Q_{\mathrm{tr}}^4+8Q_{\mathrm{tr}}^2p_{\mathrm{T}}^2+5p_{\mathrm{T}}^4}{(x_1x_2s)^2}\right.$$
$$-2Q_{\mathrm{tr}}^2\frac{5Q_{\mathrm{tr}}^4+6Q_{\mathrm{tr}}^2p_{\mathrm{T}}^2-3p_{\mathrm{T}}^4}{(x_1x_2s)^3}+Q_{\mathrm{tr}}^4\frac{8Q_{\mathrm{tr}}^4+8Q_{\mathrm{tr}}^2p_{\mathrm{T}}^2+5p_{\mathrm{T}}^4}{(x_1x_2s)^4}-4Q_{\mathrm{tr}}^8\frac{Q_{\mathrm{tr}}^2+p_{\mathrm{T}}^2}{(x_1x_2s)^5}$$
$$\left.+\frac{Q_{\mathrm{tr}}^{12}}{(x_1x_2s)^6}\right], \tag{2.12}$$

$$\left.\frac{\mathrm{d}^2\hat{\sigma}}{\mathrm{d}p_{\mathrm{T}}\mathrm{d}\eta}\right|_{D14} = \frac{3\alpha_s^3}{256\pi^2\Lambda^6}\frac{(x_1x_2s)^3}{(Q_{\mathrm{tr}}^2-x_1x_2s)^2}\frac{Q_{\mathrm{tr}}\sqrt{Q_{\mathrm{tr}}^2-4m_{\mathrm{DM}}^2}}{p_{\mathrm{T}}}\left[1-4\frac{Q_{\mathrm{tr}}^2}{x_1x_2s}+\frac{8Q_{\mathrm{tr}}^4+8Q_{\mathrm{tr}}^2p_{\mathrm{T}}^2+5p_{\mathrm{T}}^4}{(x_1x_2s)^2}\right.$$
$$-2Q_{\mathrm{tr}}^2\frac{5Q_{\mathrm{tr}}^4+6Q_{\mathrm{tr}}^2p_{\mathrm{T}}^2-3p_{\mathrm{T}}^4}{(x_1x_2s)^3}+Q_{\mathrm{tr}}^4\frac{8Q_{\mathrm{tr}}^4+8Q_{\mathrm{tr}}^2p_{\mathrm{T}}^2+5p_{\mathrm{T}}^4}{(x_1x_2s)^4}-4Q_{\mathrm{tr}}^8\frac{Q_{\mathrm{tr}}^2+p_{\mathrm{T}}^2}{(x_1x_2s)^5}$$
$$\left.+\frac{Q_{\mathrm{tr}}^{12}}{(x_1x_2s)^6}\right]. \tag{2.13}$$

The reader can find the details of the derivation of eqs. (2.5)–(2.13) in appendix A. As for the other operators, we get

$$\left.\frac{\mathrm{d}^2\hat{\sigma}}{\mathrm{d}p_{\mathrm{T}}\mathrm{d}\eta}\right|_{D2'} = \left.\frac{\mathrm{d}^2\hat{\sigma}}{\mathrm{d}p_{\mathrm{T}}\mathrm{d}\eta}\right|_{D4'} \qquad \left.\frac{\mathrm{d}^2\hat{\sigma}}{\mathrm{d}p_{\mathrm{T}}\mathrm{d}\eta}\right|_{D3'} = \left.\frac{\mathrm{d}^2\hat{\sigma}}{\mathrm{d}p_{\mathrm{T}}\mathrm{d}\eta}\right|_{D1'} \qquad \left.\frac{\mathrm{d}^2\hat{\sigma}}{\mathrm{d}p_{\mathrm{T}}\mathrm{d}\eta}\right|_{D6} = \left.\frac{\mathrm{d}^2\hat{\sigma}}{\mathrm{d}p_{\mathrm{T}}\mathrm{d}\eta}\right|_{D8} \tag{2.14}$$

$$\left.\frac{\mathrm{d}^2\hat{\sigma}}{\mathrm{d}p_{\mathrm{T}}\mathrm{d}\eta}\right|_{D7} = \left.\frac{\mathrm{d}^2\hat{\sigma}}{\mathrm{d}p_{\mathrm{T}}\mathrm{d}\eta}\right|_{D5} \qquad \left.\frac{\mathrm{d}^2\hat{\sigma}}{\mathrm{d}p_{\mathrm{T}}\mathrm{d}\eta}\right|_{D9} = \left.\frac{\mathrm{d}^2\hat{\sigma}}{\mathrm{d}p_{\mathrm{T}}\mathrm{d}\eta}\right|_{D10}, \tag{2.15}$$

in the limit of massless light quarks. The operators $D1$–$D4$ are simply related to $D1'$–$D4'$ by a straightforward rescaling

$$\left.\frac{\mathrm{d}^2\hat{\sigma}}{\mathrm{d}p_{\mathrm{T}}\mathrm{d}\eta}\right|_{D1,D2,D3,D4} = \left(\frac{m_q}{\Lambda}\right)^2\left.\frac{\mathrm{d}^2\hat{\sigma}}{\mathrm{d}p_{\mathrm{T}}\mathrm{d}\eta}\right|_{D1',D2',D3',D4'}. \tag{2.16}$$

We checked that the differences between the cross sections for $D1'$–$D4'$ computed for $m_q \neq 0$ and those reported above assuming $m_q = 0$ are at the per-mille level, so the approximation $m_q = 0$ which we used in all our analytical calculations is justified. The cross sections for the UV completions of dim-6 operators, with $s$-channel exchange of a mediator of mass $M_{\mathrm{med}}$, are simply obtained by the replacement $1/\Lambda^4 \to g_q^2 g_\chi^2/[Q_{\mathrm{tr}}^2 - M_{\mathrm{med}}^2]^2$.



JCAP06(2014)060

In order to get the cross sections initiated by the colliding protons one needs to average over the PDFs. For example, for processes with initial state quarks

$$\left.\frac{\mathrm{d}^2\sigma}{\mathrm{d}p_{\mathrm{T}}\mathrm{d}\eta}\right|_{Di} = \sum_q \int \mathrm{d}x_1\mathrm{d}x_2[f_q(x_1)f_{\bar{q}}(x_2) + f_q(x_2)f_{\bar{q}}(x_1)] \left.\frac{\mathrm{d}^2\hat{\sigma}}{\mathrm{d}p_{\mathrm{T}}\mathrm{d}\eta}\right|_{Di} . \tag{2.17}$$

We have performed the analytical calculation only for the emission of an initial state gluon (identified with the final jet observed experimentally). The extension to include also the smaller contribution coming from initial radiation of quarks ($qg \to \chi\chi{+}q$) is done numerically in section 3.

### 2.2 Results and discussion

In what regions of the parameter space $(\Lambda, m_{\mathrm{DM}})$ is the effective description accurate and reliable? The truncation to the lowest-dimensional operator of the EFT expansion is accurate only if the momentum transfer is smaller than an energy scale of the order of $\Lambda$, see eqs. (1.5). Therefore we want to compute the fraction of events with momentum transfer lower than the EFT cutoff scale. To this end we define the ratio of the cross section obtained in the EFT with the requirement $Q_{\mathrm{tr}} < \Lambda$ on the PDF integration domain, over the total cross section obtained in the EFT.

$$R_\Lambda^{\mathrm{tot}} \equiv \frac{\sigma|_{Q_{\mathrm{tr}}<\Lambda}}{\sigma} = \frac{\int_{p_{\mathrm{T}}^{\mathrm{min}}}^{p_{\mathrm{T}}^{\mathrm{max}}} \mathrm{d}p_{\mathrm{T}} \int_{-2}^{2} \mathrm{d}\eta \left.\frac{\mathrm{d}^2\sigma}{\mathrm{d}p_{\mathrm{T}}\mathrm{d}\eta}\right|_{Q_{\mathrm{tr}}<\Lambda}}{\int_{p_{\mathrm{T}}^{\mathrm{min}}}^{p_{\mathrm{T}}^{\mathrm{max}}} \mathrm{d}p_{\mathrm{T}} \int_{-2}^{2} \mathrm{d}\eta \frac{\mathrm{d}^2\sigma}{\mathrm{d}p_{\mathrm{T}}\mathrm{d}\eta}}. \tag{2.18}$$

To sum over the possible $p_{\mathrm{T}}, \eta$ of the jets, we integrate the differential cross sections over values typically considered in the experimental searches. We consider $p_{\mathrm{T}}^{\mathrm{min}} = 500\,\mathrm{GeV}$ (as used in the signal region SR4 of [12]), $|\eta| < 2$ and the two cases with center-of-mass energies $\sqrt{s} = 8$ TeV and 14 TeV. For $p_{\mathrm{T}}^{\mathrm{max}}$ we used 1, 2 TeV for $\sqrt{s} = 8, 14$ TeV, respectively. The sum over quark flavours is performed only considering $u, d, c, s$ quarks.

We first study the behavior of the ratio $R_\Lambda^{\mathrm{tot}}$, as a function of $\Lambda$ and $m_{\mathrm{DM}}$ The results are shown in figure 1. We show only results for representative operators $D1', D5, D9$. This ratio $R_\Lambda^{\mathrm{tot}}$ gets closer to unity for large values of $\Lambda$, as in this case the effect of the cutoff becomes negligible. The ratio drops for large $m_{\mathrm{DM}}$ because the momentum transfer increases in this regime. This confirms our precedent analysis of ref. [29], that the EFT works better for large $\Lambda$ and small $m_{\mathrm{DM}}$. Notice also that, going from $\sqrt{s} = 8$TeV to $\sqrt{s} = 14$TeV, the results scale almost linearly with the energy, so for the same value of the ratio $m_{\mathrm{DM}}/\Lambda$ one obtains nearly the same $R_\Lambda^{\mathrm{tot}}$.

Next, we turn to study the contours of constant values of the quantity $R_\Lambda^{\mathrm{tot}}$, in the plane $(m_{\mathrm{DM}}, \Lambda)$. These contour curves for the different operators are shown in figure 2 for $\sqrt{s} = 8$ TeV and in figure 3 for $\sqrt{s} = 14$ TeV. The requirement that at least 50% of the events occur with momentum transfer below the cutoff scale $\Lambda$ requires such a cutoff scale to be above $\sim 1$TeV for $\sqrt{s} = 8\,\mathrm{TeV}$, or above $\sim 2$TeV for $\sqrt{s} = 14\,\mathrm{TeV}$. Note also that the contours for $D1$–$D4$ differ by the corresponding contours for $D1'$–$D4'$ by $\mathcal{O}(1)$ factors, due to the different weighting of the quarks' PDFs. On the other hand, the experimental bounds on the scale of the operators $D1$–$D4$ are much lower (of the order of tens of GeV), as such operators experience an additional suppression of $m_q/\Lambda$. This means that the bounds on $D1$–$D4$ are not reliable from the point of view of EFT validity.

We stress once again that the precise definition of a cutoff scale for an EFT is only possible when the details of the UV completion are known. The most conservative regime is



JCAP06(2014)060

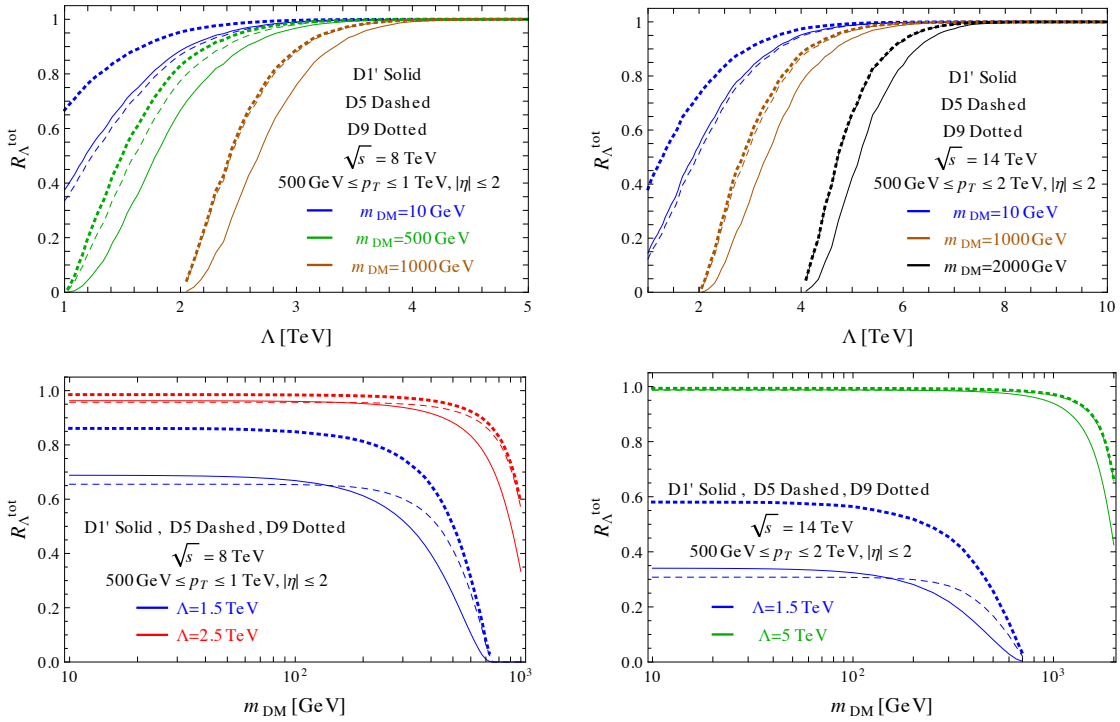


**Figure 1**. The ratio $R_\Lambda^{\rm tot}$ defined in eq. (2.18) for operators $D1'$ (solid lines), $D5$ (dashed lines) and $D9$ (dotted lines) as a function of $\Lambda$ and $m_{\rm DM}$, for $\sqrt{s} = 8\,\text{TeV}$ (left panel) and $14\,\text{TeV}$ (right panel).

when the couplings of the UV theory reach their maximal values allowed by perturbativity. In such a situation, the requirement on the momentum transfer becomes $Q_{\rm tr} < 4\pi\Lambda$. We show the effect of varying the cutoff scale in figure 4, for the representative contour $R_\Lambda^{\rm tot} = 50\%$ of D5. As it should be clear, the variation of the cutoff scale is equivalent to a change of the unknown couplings of the UV theory. All the operators have very similar results, as the contours scale linearly with the cutoff. As a comparison, we show as a shaded area the region $\Lambda > m_{\rm DM}/(2\pi)$ often used as a benchmark for the validity of the EFT (see eq. (1.4)). The 50% contour is above such a region, meaning that the parameter space regions of validity of the effective operator approach is smaller than commonly considered.

To close this section let us comment on another question one may ask: what is the difference between interpreting data with an effective operator and with its simplest UV completion? This question has already been addressed in ref. [29] for the operator $D1'$, by studying the ratio of the cross sections obtained with the UV theory and with the effective operator. For each of the operators in table 1 one can write a simple UV-complete Lagrangian, see e.g. eqs. (2.1)–(2.2). The very same analysis can be repeated for all the other operators and we checked that the same qualitative conclusions can be drawn. In particular, if $\Lambda$ is not larger than a few TeV, interpreting the experimental data in terms of EFT or in terms of a simplified model with a mediator can make a significant difference.

## 3 Comparison with MonteCarlo simulations

In order to perform an alternative check of our analytical results and to be able to compare to the experimental limits as close as possible, we present in this section the results of numerical event simulations.



JCAP06(2014)060

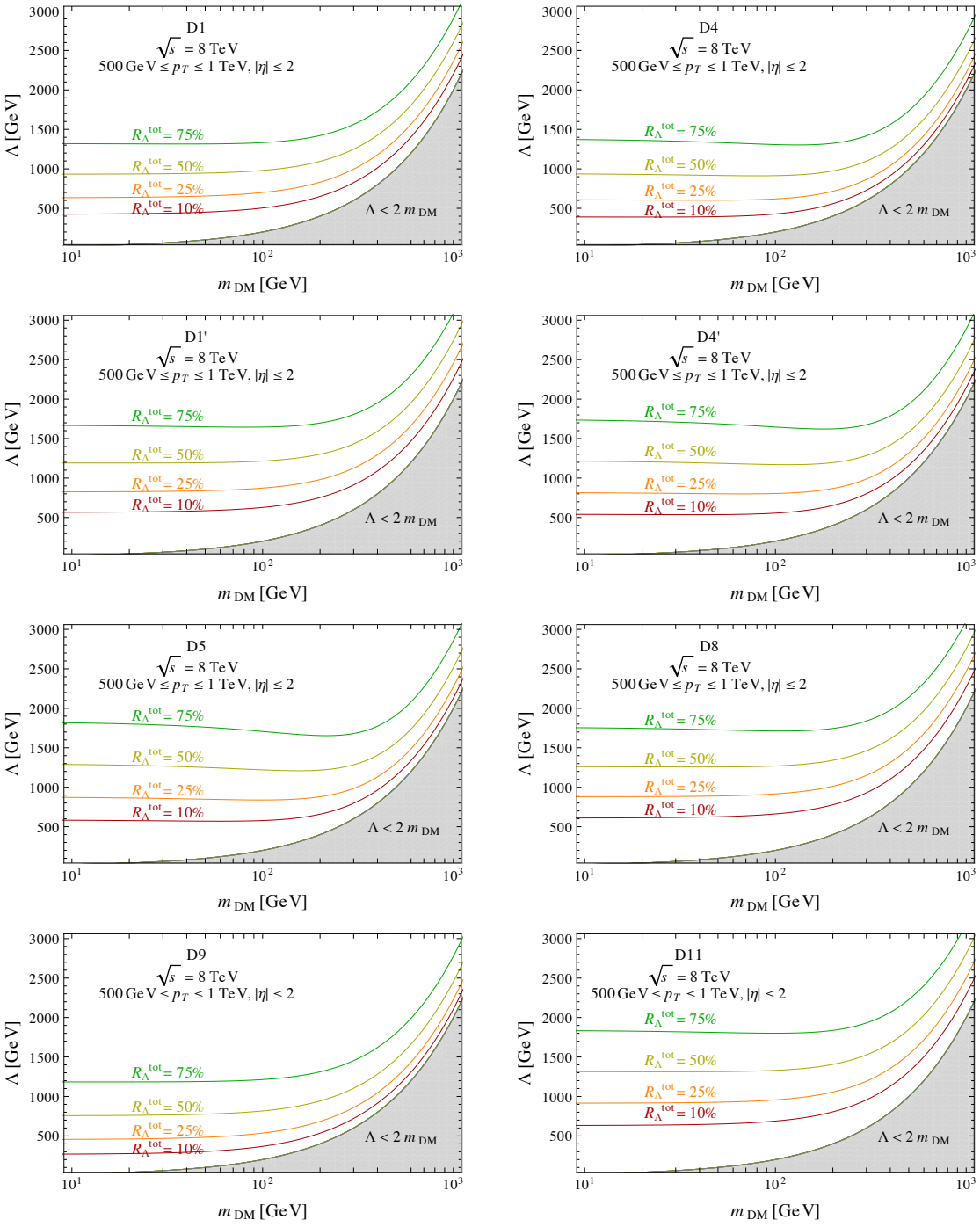


**Figure 2**. Contours for the ratio $R_\Lambda^{\rm tot}$, defined in eq. (2.18), on the plane $(m_{\rm DM}, \Lambda)$, for the different operators. We set $\sqrt{s} = 8\text{TeV}$, $|\eta| \leq 2$ and $500\,\text{GeV} < p_{\rm T} < 1\text{TeV}$.

JCAP06(2014)060

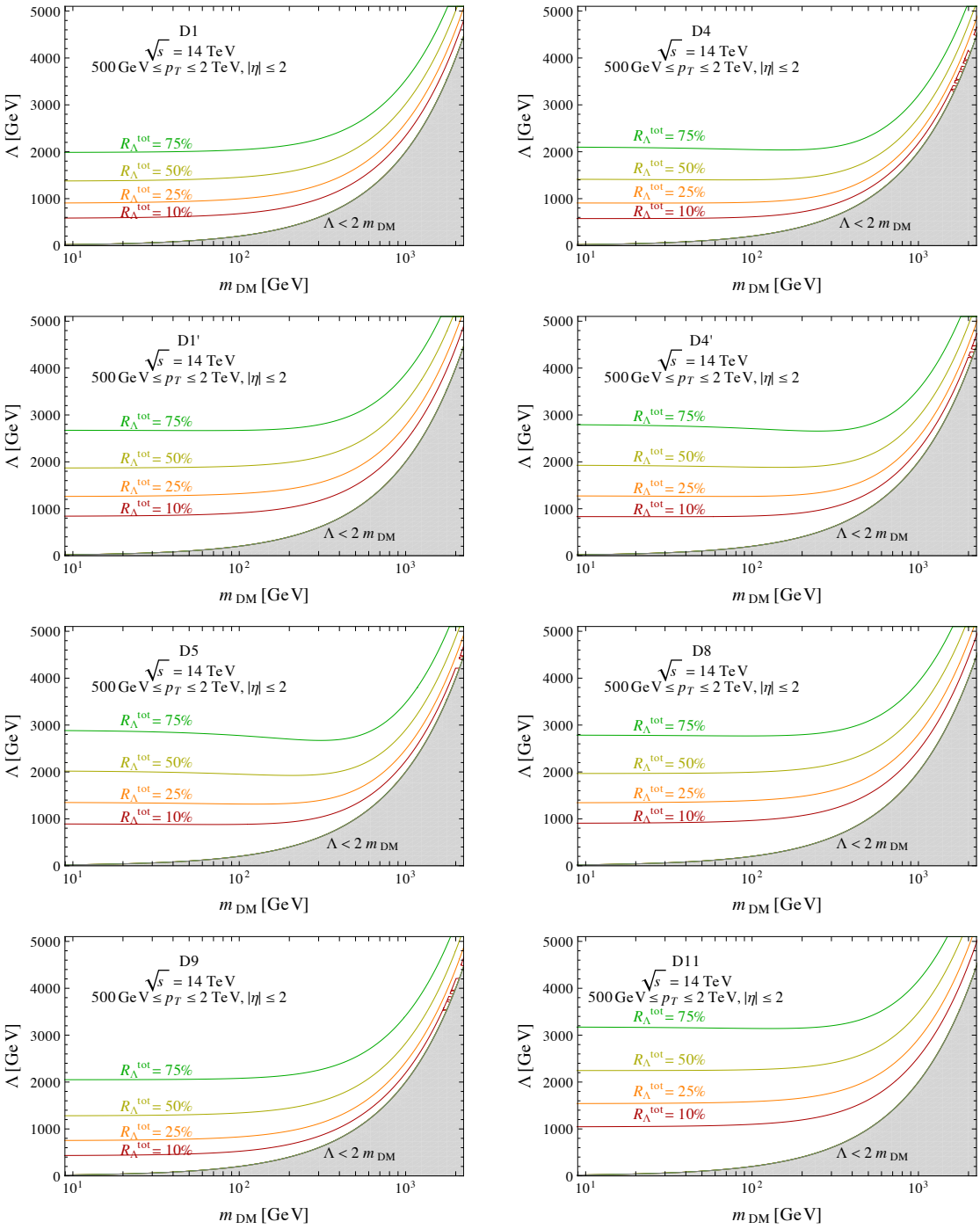


**Figure 3**. Contours for the ratio $R_\Lambda^{\rm tot}$, defined in eq. (2.18), on the plane $(m_{\rm DM}, \Lambda)$, for the different operators. We set $\sqrt{s} = 14$TeV, $|\eta| \leq 2$ and $500\,{\rm GeV} < p_{\rm T} < 2$TeV.

JCAP06(2014)060

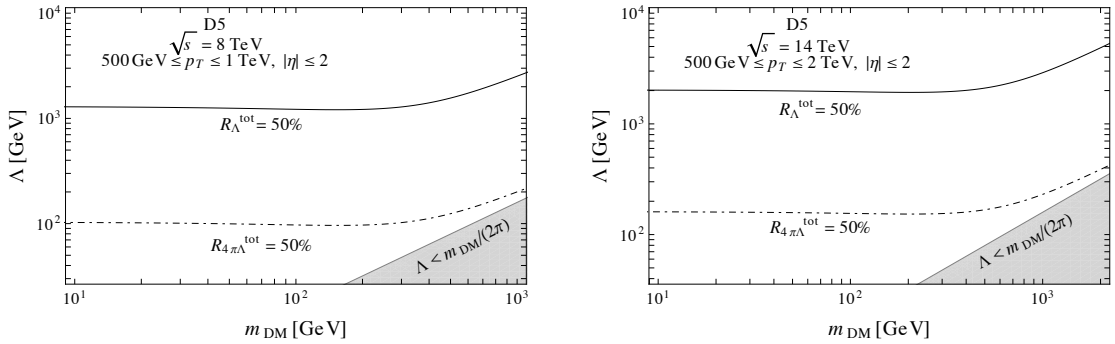


**Figure 4**. 50% contours for the ratio $R_\Lambda^{\rm tot}$ for the operator $D5$, varying the cutoff $Q_{\rm tr} < \Lambda$ (solid line) and $Q_{\rm tr} < 4\pi\Lambda$ (dot-dashed line). We have also shown the region corresponding to $\Lambda < m_{\rm DM}/(2\pi)$ (gray shaded area), often used as a benchmark for the validity of the EFT. We set $\sqrt{s} = 8$ TeV (left panel) and $\sqrt{s} = 14$ TeV (right panel).

### 3.1 Simulation and analysis description

We made use of MadGraph 5 [38] to simulate $pp$ collisions at $\sqrt{s} = 8$ TeV and $\sqrt{s} = 14$ TeV. Both PDF sets CTEQ6L1 and MSTW2008LO (discussed in refs. [39, 40]) are employed. The PDF choice affects the cross section, but only minimally the acceptance. Hence, the change in contours of $R_\Lambda^{\rm tot}$ is negligible. Since MSTW2008LO is used for the analytical calculations, this set is also used where direct comparisons between simulation and calculation are shown. For the comparison to the experimental results, CTEQ6L1 is used instead. Only $u, d, c, s$ quarks were considered, both in the initial and in the final state.

According to the event kinematics we have evaluated whether or not the conditions of validity discussed in section 2 are fulfilled. Specifically, we have checked if eqs. (1.3) and (1.4) are fulfilled, that is, if the following condition is satisfied

$$\Lambda > \frac{Q_{\rm tr}}{\sqrt{g_q g_\chi}} > 2\frac{m_{\rm DM}}{\sqrt{g_q g_\chi}}\,. \tag{3.1}$$

Samples of 20000 events were simulated for each operator, scanning DM mass values of 10, 50, 80, 100, 400, 600, 800 and 1000 GeV and cutoff scales of 250, 500, 1000, 1500, 2000, 2500 and 3000 GeV in the case of $\sqrt{s} = 8$ TeV collisions. When increasing the collision energy to $\sqrt{s} = 14$ TeV, the DM mass of 2000 GeV and cutoff scales of 4000 and 5000 GeV were added.

From the simulated samples the fraction of events fulfilling $\Lambda > Q_{\rm tr}/\sqrt{g_q g_\chi}$ for each pair of DM mass and cutoff scale can be evaluated, if one assumes a certain value for the couplings $\sqrt{g_\chi g_q}$ connecting the cutoff scale $\Lambda$ and the mediator mass $M$ via $\Lambda = M/\sqrt{g_q g_\chi}$. As above, $g_q g_\chi$ was assumed to be 1.

### 3.2 Results

In order to confirm that analytical and numerical results are in agreement, figure 5 shows a comparison for the operators $D1'$, $D4'$, $D5$, $D8$ and $D9$. The results were obtained for the scenario of one radiated gluon jet above 500 GeV within $|\eta| < 2$. The contours of $R_\Lambda^{\rm tot} = 50\%$ from analytical and numerical evaluation agree within less than 7 %. The remaining differences could be due to the upper jet $p_{\rm T}$ cut not imposed during event simulation but needed for the analytical calculation, and the details of the fitting procedures.



JCAP06(2014)060

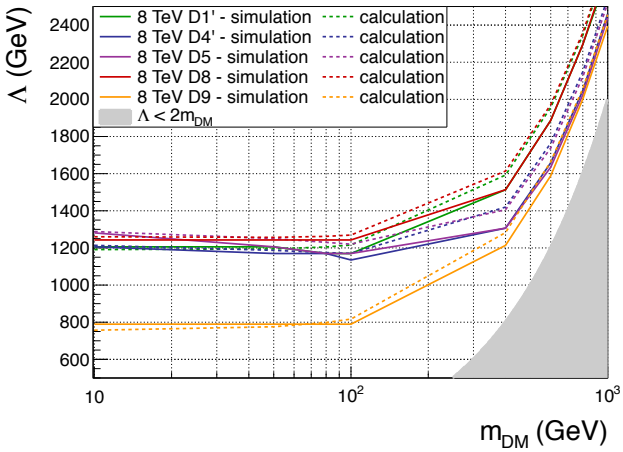


**Figure 5**. Comparison of the contour $R_\Lambda^{\text{tot}} = 50\%$ for the analytical calculation (dashed line) and the simulation (solid line) for the different operators $D1'$, $D4'$, $D5$, $D8$ and $D9$. The results agree within less than 7 %.

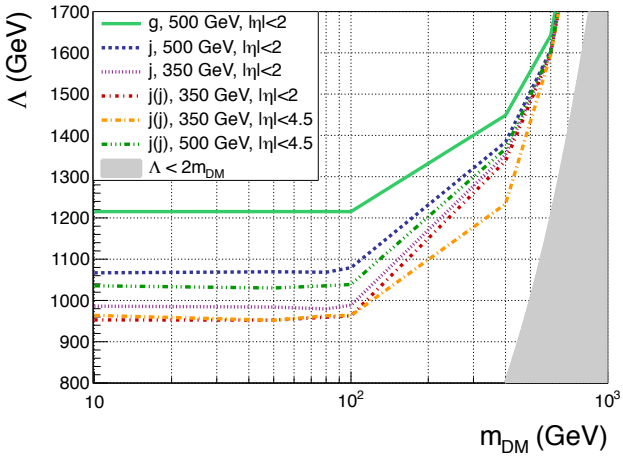


**Figure 6**. The changes of the contour of $R_\Lambda^{\text{tot}} = 50\%$ are shown for several variations from the analytically calculated scenario to a scenario close to the cuts used in the ATLAS monojet analysis exemplarily for the operator $D5$ at $\sqrt{s} = 8\,\text{TeV}$. In the legend, "g" means only gluon radiation, "j" stands for either quark- or gluon-initiated jets, "j(j)" means a second jet is allowed.

Next, we vary the kinematical constraints step by step from the scenario considered in the analytical calculations, namely one radiated gluon jet above 500 GeV within $|\eta| < 2$, to a scenario closest to the analysis cuts applied in the ATLAS monojet analysis [12]. More specifically, the leading jet is allowed to come from either a gluon or a quark being radiated, the leading jet $p_{\text{T}}$ cut is changed from 500 GeV to 350 GeV, a second jet is allowed and its range in $\eta$ is enlarged to $|\eta| < 4.5$. No further cuts are applied at simulation level.

The effect of the variation of the cuts can be seen in figure 6. Allowing not only for a gluon jet but also taking into account the possibility of a quark jet changes the $R_\Lambda^{\text{tot}}$ contours appreciably. The change from lowering the $p_{\text{T}}$ of the leading jet has a smaller effect. Allowing for a second jet and enhancing its rapidity range barely changes the $R_\Lambda^{\text{tot}}$ contour, especially at large $m_{\text{DM}}$ values.



JCAP06(2014)060

| $\sqrt{s} = 8$ TeV | | | | | |
|---|---|---|---|---|---|
| Operator | a | b | c | d | e |
| D1 | 1.32 | 787.13 | 1.39 | 1.08 | 1.53 |
| D1' | 1.30 | 1008.25 | 1.49 | 0.77 | 1.83 |
| D4 | 1.65 | 702.93 | 1.14 | 0.65 | 1.75 |
| D4' | 1.51 | 859.83 | 1.22 | 0.48 | 1.92 |
| D5 | 1.54 | 816.83 | 1.18 | 0.50 | 1.85 |
| D8 | 1.23 | 964.62 | 1.50 | 0.91 | 1.59 |
| D9 | 1.43 | 681.92 | 1.15 | 1.02 | 1.35 |
| D11 | 1.23 | 1002.33 | 1.49 | 0.82 | 1.69 |

| $\sqrt{s} = 14$ TeV | | | | | |
|---|---|---|---|---|---|
| Operator | a | b | c | d | e |
| D1 | 0.89 | 1017.37 | 1.45 | 1.28 | 1.24 |
| D1' | 0.43 | 909.66 | 1.59 | 0.53 | 1.37 |
| D4 | 1.23 | 996.82 | 1.25 | 0.80 | 1.48 |
| D4' | 0.76 | 982.75 | 1.33 | 0.37 | 1.63 |
| D5 | 0.78 | 894.86 | 1.25 | 0.39 | 1.54 |
| D8 | 0.48 | 945.09 | 1.55 | 0.74 | 1.24 |
| D9 | 0.91 | 891.65 | 1.21 | 1.23 | 1.04 |
| D11 | 0.68 | 1250.49 | 1.58 | 0.81 | 1.35 |

**Table 2**. Coefficient for the fitting functions for $R_\Lambda^{\rm tot}$ in eq. (3.2), in the cases $\sqrt{s} = 8$ and 14 TeV. The fitting functions describe processes where quarks and/or gluons are radiated, the final state contains 1 or 2 jets, where the leading jet has minimum $p_{\rm T}$ of 350 GeV while the second jet is allowed to be within $|\eta| < 4.5$. See text for further details.

If the collision energy is augmented to $\sqrt{s} = 14$ TeV, all the $R_\Lambda^{\rm tot}$ contours increase. As seen for $\sqrt{s} = 8$ TeV, moving to the scenario closer to the experimental analysis leads to contours that are at most $\sim 30\%$ lower in $\Lambda$.

After having extracted $R_\Lambda^{\rm tot}$ for each WIMP and mediator mass, a curve can be fitted through the points obtained in the plane of $R_\Lambda^{\rm tot}$ and $\Lambda$. The following functional form is used for this purpose

$$R_\Lambda^{\rm tot} = \left[1 - e^{-a\left(\frac{\Lambda - 2m_{\rm DM}}{b}\right)^c}\right]\left[1 - e^{-d\left(\frac{\Lambda + 2m_{\rm DM}}{b}\right)^e}\right] . \tag{3.2}$$

Further, the parameters are fitted for each DM mass separately. From these fits, the points denoting a cutoff scale where $R_\Lambda^{\rm tot}$ equals e.g. 50% can be extracted for each DM mass, and the lines of constant $R_\Lambda^{\rm tot}$ can be plotted in the usual limit-setting plane $\Lambda$ vs. $m_{\rm DM}$. Table 2 collects the values of the fitting parameters for all operators except D12-D14, for which no experimental analysis exists.

## 4 Implications of the limited validity of EFT in DM searches at LHC

Figure 7 shows the experimental limits obtained from the ATLAS monojet analysis [12] in the plane ($\Lambda$, $m_{\rm DM}$), for the opearators D5, D8 and D11. The contours of $R_\Lambda^{\rm tot}$ for 25%, 50% and 75% are superimposed. The experimental limits are placed in a region where about 30% of the events can be expected to fulfill the EFT conditions — the exact number depends on the operator considered. Especially the limit on the gluon operator $D11$ seems questionnable. For comparison, dashed lines show the contours of $R_\Lambda^{\rm tot}$ for the extreme case of couplings $\sqrt{g_q g_\chi} = 4\pi$, presenting the limiting case for which the theory is still considered perturbative.

Unfortuntately, there is no possibility to measure $Q_{\rm tr}$ in data, on an event-by-event basis. So the information on what is the fraction of the events to cut out comes from analytical computations or a numerical simulation, as we explained in this paper. To assess the impact of the limited validity of the EFT on the current collider bounds, we adopt the procedure that relies on the assumption that the $p_{\rm T}$ (or MET) distributions with the $Q_{\rm tr}$ cut are simply a rescaling of those without the cut. A more refined study should account for



JCAP06(2014)060

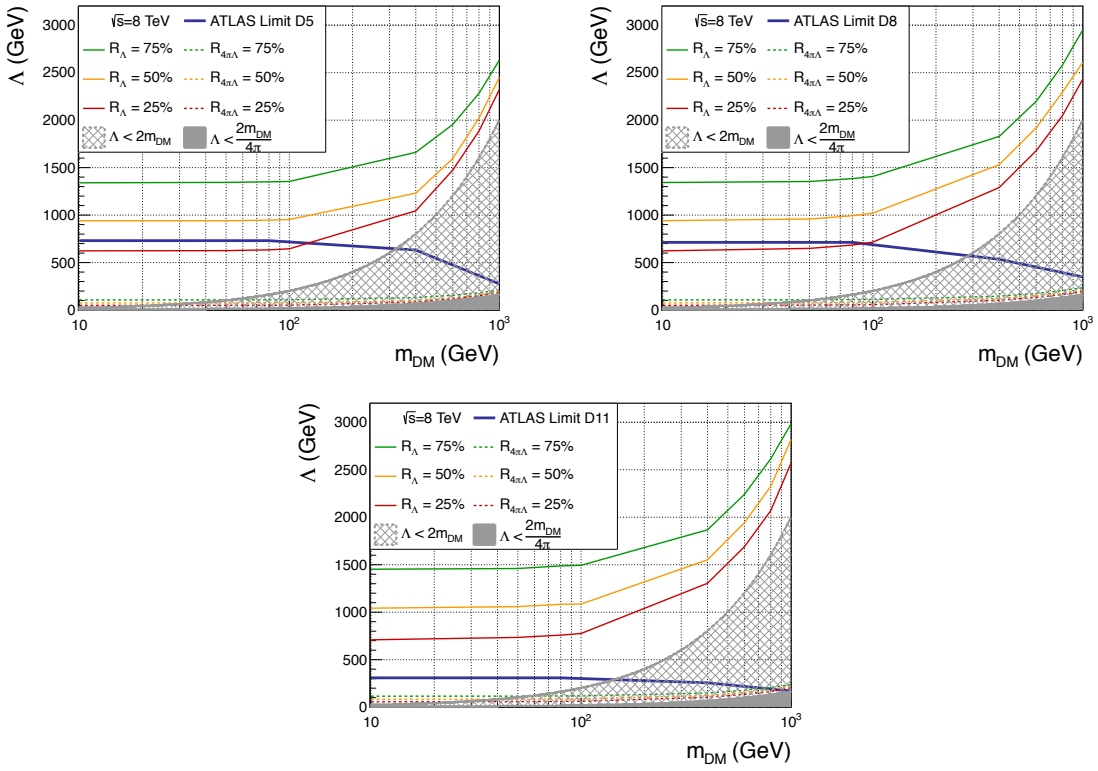


**Figure 7**. 25%, 50% and 75% contours for the ratio $R_\Lambda^{\rm tot}$, compared to the experimental limits from ATLAS [12] (blue line). Also indicated are the contours of $R_\Lambda^{\rm tot}$ in the extreme case when setting the couplings $\sqrt{g_q g_\chi} = 4\pi$ (dashed lines). Results are shown for different operators: D5 (upper left panel), D8 (upper right panel) and D11 (lower panel).

possible kinematic shape changes with the jet transverse momentum and/or missing energy and DM mass.[2]

Very naively, neglecting the statistical and systematical uncertainties, the number of signal events in a given EFT model has to be less than the experimental observation, $N_{\rm signal}(\Lambda, m_{\rm DM}) < N_{\rm expt}$. The cross section due to an operator of mass dimension $d$ scale like $\Lambda^{-2(d-4)}$, so $N_{\rm signal}(\Lambda, m_{\rm DM}) = \Lambda^{-2(d-4)} \tilde{N}_{\rm signal}(m_{\rm DM})$, and the experimental lower bound in the scale of the operator becomes

$$\Lambda > \left[\tilde{N}_{\rm signal}(m_{\rm DM})/N_{\rm exp}\right]^{1/[2(d-4)]} \equiv \Lambda_{\rm expt.}\,. \tag{4.1}$$

Now, if we do not consider any information about the shapes of the $p_{\rm T}$ or MET distributions, the experimental bound only comes from the total number of events passing given cuts. The fact that a fraction of the events involve a transfer momentum exceeding the cutoff scale of the EFT means that the number of signal events for placing a limit gets reduced by a factor $R_\Lambda^{\rm tot}$. Therefore, actually $N_{\rm signal}(\Lambda, m_{\rm DM}) \to R_\Lambda^{\rm tot}(m_{\rm DM}) N_{\rm signal}(\Lambda, m_{\rm DM})$, so the new limit is found by solving the implicit equation

$$\Lambda > [R_\Lambda^{\rm tot}(m_{\rm DM})]^{1/2[(d-4)]} [N_{\rm signal}(m_{\rm DM})/N_{\rm exp}]^{1/[2(d-4)]} = [R_\Lambda^{\rm tot}(m_{\rm DM})]^{1/[2(d-4)]} \Lambda_{\rm expt} \tag{4.2}$$

[2]Preliminary studies indicate that the method adopted in this paper is quite reasonable for cuts with $Q_{\rm tr} < 750\,{\rm GeV}$ or weaker [41].



JCAP06(2014)060

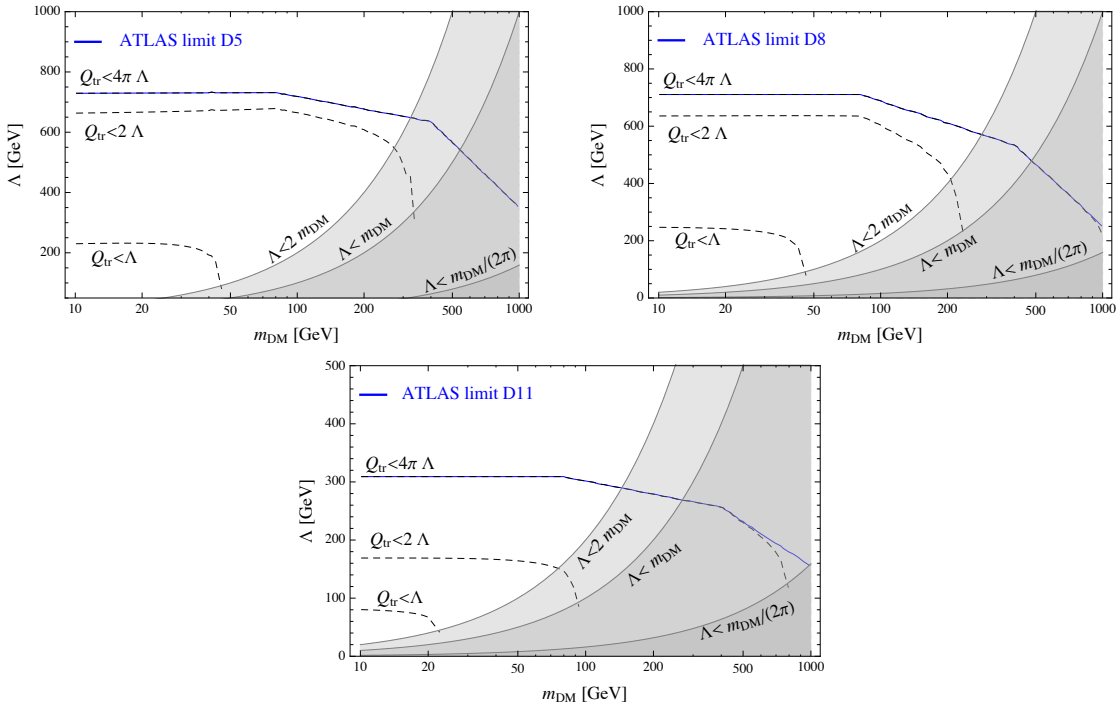


**Figure 8**. The experimental limits by ATLAS [12] on the suppression scale $\Lambda$ are shown as solid blue lines. The updated limits taking into account EFT validity are shown as dashed black lines, for $Q_{\rm tr} < \Lambda, 2\Lambda, 4\pi\Lambda$, corresponding to different choices of the UV couplings: $\sqrt{g_q g_\chi} = 1, 2, 4\pi$, respectively. The corresponding kinematical constraints (eq. (3.1)) are denoted by gray bands. The different plots refer to different operators: D5 (upper left panel), D8 (upper right panel) and D11 (lower panel).

and it turns out to be weaker than $\Lambda_{\rm expt}$. In figure 8 we show the new limits for the dim-6 operators D5, D8 and the dim-7 operator D11, for the conditions $Q_{\rm tr} < \Lambda, 2\Lambda, 4\pi\Lambda$, corresponding different choices of the UV couplings: $\sqrt{g_q g_\chi} = 1, 2, 4\pi$, respectively. The curves are obtained solving eq. (4.2) with $R^{\rm tot}_{\Lambda}, R^{\rm tot}_{2\Lambda}, R^{\rm tot}_{4\pi\Lambda}$ respectively. The ATLAS bound reported is the 90%CL observed limit. The functions $R^{\rm tot}_{\Lambda}$ used are taken from the fitting functions described in table 2, which include both quark and gluon jets, and the same cuts as the "Signal Region 3" used by ATLAS. As expected, the weaker is the condition on $Q_{\rm tr}$, the more the new limits approach the ATLAS bound. In the case of extreme couplings $\sqrt{g_q g_\chi} = 4\pi$, the condition on the momentum transfer is very conservative $Q_{\rm tr} < 4\pi\Lambda$. For D5 and D8, the new limit is indisinguishable from the ATLAS one, meaning that the experimental results are safe from the EFT point of view, in this limiting situation. For D11, even for extreme values of the couplings, the bound at large DM masses must be corrected. In general, for couplings of order one, the limits which are safe from the EFT point of view are appreciably weaker than those reported. We encourage the experimental collaborations to take this point into account when publishing their limits.

## 5 Conclusions

The search for DM is one of the main targets of LHC analyses. In this paper we have continued our previous investigation to assess the validity of the EFT commonly used in interpreting



JCAP06(2014)060

such searches. Following ref. [29], we have studied the quantity $R_\Lambda^{\rm tot}$ (see eq. (2.18), which quantifies the error made when using effective operators to describe processes with very high momentum transfer. Our criterion indicates up to what cutoff energy scale the effective description is valid, depending on the DM mass and couplings. We have performed the analysis for the full list of EFT operators, connecting fermion DM particles and quarks or gluons, used by the ATLAS and CMS collaborations and originated from the exchange of heavy mediators in the $s$-channel. We have also extended our analysis to the case of $\sqrt{s} = 14$ TeV. Furthermore, we have validated our analytical results by performing numerical event simulations which reproduce the experimental situation in the closest possible way. Our results indicate that the range of validity of the EFT is significantly limited in the parameter space $(\Lambda, m_{\rm DM})$. While our findings are valid for the $s$-channel, a similar analysis is under way for the $t$-channel [42] where similar results are obtained.

Does it mean that the EFT is not the best tool to interpret the current LHC data of DM searches? The answer is yes and no. On the negative side, our results clearly cry out for an overcoming of the EFT, most possibly through identifying a handful of classes of models (able to reproduce the EFT operators in the heavy mediator limit); this would allow a consistent analysis of the current and future LHC data by consistently taking into account the role played by the mediator. On the positive side, keep working with the EFT allows to avoid the overwhelming model-dependence generated by the many DM models proposed so far. Nonetheless, as we have shown in section 4, the price to pay is a deterioration of the limits presented so far.


## Acknowledgments

We thank A. Brennan, C. Doglioni, G. Iacobucci, T. Jacques, S. Schramm and S. Vallecorsa for many interesting conversations. ADS acknowledges partial support from the European Union FP7 ITN INVISIBLES (Marie Curie Actions, PITN-GA-2011-289442). JG acknowledges partial support from UNIGE and SNF grant 200020-144493, "High-Energy Hadron Interactions: ATLAS at the CERN LHC".


## A Three-body cross sections

### A.1 Generalities

In this appendix we show the details of the calculations of the tree-level cross sections for the hard scattering process $f(p_1) + \bar{f}(p_2) \to \chi(p_3) + \chi(p_4) + g(k)$, where $f$ is either a quark (operators D1-D10) or a gluon (D11-D14), and the final gluon is emitted from the initial state.

The differential cross section is generically given by

$$d\hat{\sigma} = \frac{\sum \overline{|\mathcal{M}|^2}}{4(p_1 \cdot p_2)} \mathrm{d}\Phi_3 \,, \tag{A.1}$$

where the three-body phase space is

$$\mathrm{d}\Phi_3 = (2\pi)^4 \delta^{(4)}(p_1 + p_2 - p_3 - p_4 - k) \frac{\mathrm{d}\mathbf{p}_3}{(2\pi)^3 2p_3^0} \frac{\mathrm{d}\mathbf{p}_4}{(2\pi)^3 2p_4^0} \frac{\mathrm{d}\mathbf{k}}{(2\pi)^3 2k^0} \,. \tag{A.2}$$



JCAP06(2014)060

### A.2 Matrix elements

In the limit of massless light quarks, they have definite helicity and it makes no difference for the cross sections whether there is $q$ or $\gamma^5 q$ in the operator. Therefore the following identifications between pairs of operators hold:

$$D1' \leftrightarrow D3', \qquad D2' \leftrightarrow D4', \qquad D5 \leftrightarrow D7, \qquad D6 \leftrightarrow D8, \qquad D9 \leftrightarrow D10\,, \tag{A.3}$$

while the "primed" and "unprimed" operators are related as in eq. (2.16). For definiteness, we choose to work with $D1', D4', D5, D8, D9$ and $D11 - D14$.

The amplitudes are given by

$$\mathcal{M}_{D1'} = -ig_s \frac{1}{\Lambda^2}\epsilon^{*a}_\mu(k)\left[\frac{\bar v(p_2)(\not p_1 - \not k)\gamma^\mu T^a u(p_1)}{(p_1-k)^2} - \frac{\bar v(p_2)\gamma^\mu T^a(\not p_2 - \not k)u(p_1)}{(p_2-k)^2}\right]\bar u(p_3)v(p_4)\,, \tag{A.4}$$

$$\mathcal{M}_{D4'} = -ig_s \frac{1}{\Lambda^2}\epsilon^{*a}_\mu(k)\left[\frac{\bar v(p_2)\gamma^5(\not p_1 - \not k)\gamma^\mu T^a u(p_1)}{(p_1-k)^2} - \frac{\bar v(p_2)\gamma^\mu T^a(\not p_2 - \not k)\gamma^5 u(p_1)}{(p_2-k)^2}\right] \times\bar u(p_3)\gamma^5 v(p_4)\,, \tag{A.5}$$

$$\mathcal{M}_{D5} = -ig_s \frac{g_{\nu\rho}}{\Lambda^2}\epsilon^{*a}_\mu(k)\left[\frac{\bar v(p_2)\gamma^\nu(\not p_1 - \not k)\gamma^\mu T^a u(p_1)}{(p_1-k)^2} - \frac{\bar v(p_2)\gamma^\mu T^a(\not p_2 - \not k)\gamma^\nu u(p_1)}{(p_2-k)^2}\right] \times\bar u(p_3)\gamma^\rho v(p_4)\,, \tag{A.6}$$

$$\mathcal{M}_{D8} = -ig_s \frac{g_{\nu\rho}}{\Lambda^2}\epsilon^{*a}_\mu(k)\left[\frac{\bar v(p_2)\gamma^\nu\gamma^5(\not p_1 - \not k)\gamma^\mu T^a u(p_1)}{(p_1-k)^2} - \frac{\bar v(p_2)\gamma^\mu T^a(\not p_2 - \not k)\gamma^\nu\gamma^5 u(p_1)}{(p_2-k)^2}\right] \times\bar u(p_3)\gamma^\rho\gamma^5 v(p_4)\,, \tag{A.7}$$

$$\mathcal{M}_{D9} = -i\frac{g_s}{16}\frac{g_{\mu\rho}g_{\nu\sigma}}{\Lambda^2}\epsilon^{*a}_\alpha(k)\left[\frac{\bar v(p_2)\sigma^{\mu\nu}(\not p_1 - \not k)\gamma^\alpha T^a u(p_1)}{(p_1-k)^2} - \frac{\bar v(p_2)\gamma^\alpha T^a(\not p_2 - \not k)\sigma^{\mu\nu}u(p_1)}{(p_2-k)^2}\right] \times\bar u(p_3)\sigma^{\rho\sigma}v(p_4)\,, \tag{A.8}$$

$$\begin{aligned}\mathcal{M}_{D11} = {}& \frac{g_s^3}{4\pi}\frac{1}{\Lambda^3}f_{abc}\epsilon_\mu(p_1)\epsilon_\nu(p_2)\epsilon^*_\rho(k)\bar u(p_3)v(p_4)\\ &\Bigg[\frac{(g^{\mu\sigma}(2p_1-k)^\rho + g^{\rho\sigma}(2k-p_1)^\mu - g^{\mu\rho}(k+p_1)^\sigma)((p_1-k)^\nu p_{2\sigma} - (p_1-k)\cdot p_2 g^\nu_\sigma)}{(p_1-k)^2}\\ &-\frac{(g^{\nu\sigma}(2p_2-k)^\rho + g^{\rho\sigma}(2k-p_2)^\nu - g^{\nu\rho}(k+p_2)^\sigma)((p_2-k)^\mu p_{1\sigma} - (p_2-k)\cdot p_1 g^\mu_\sigma)}{(p_2-k)^2}\\ &-\frac{(g^{\mu\nu}(p_1-p_2)^\sigma + g^{\nu\sigma}(p_1+2p_2)^\mu - g^{\mu\sigma}(2p_1+p_2)^\nu)((p_1+p_2)^\rho k_\sigma - k\cdot(p_1+p_2)g^\rho_\sigma)}{(p_1+p_2)^2}\\ &+g^{\mu\nu}(p_1-p_2)^\rho + g^{\nu\rho}(p_2+k)^\mu - g^{\mu\rho}(k+p_1)^\nu\Bigg]\,,\end{aligned} \tag{A.9}$$

$$\begin{aligned}\mathcal{M}_{D12} = {}& i\frac{g_s^3}{4\pi}\frac{1}{\Lambda^3}f_{abc}\epsilon_\mu(p_1)\epsilon_\nu(p_2)\epsilon^*_\rho(k)\bar u(p_3)\gamma^5 v(p_4)\\ &\Bigg[\frac{(g^{\mu\sigma}(2p_1-k)^\rho + g^{\rho\sigma}(2k-p_1)^\mu - g^{\mu\rho}(k+p_1)^\sigma)((p_1-k)^\nu p_{2\sigma} - (p_1-k)\cdot p_2 g^\nu_\sigma)}{(p_1-k)^2}\\ &-\frac{(g^{\nu\sigma}(2p_2-k)^\rho + g^{\rho\sigma}(2k-p_2)^\nu - g^{\nu\rho}(k+p_2)^\sigma)((p_2-k)^\mu p_{1\sigma} - (p_2-k)\cdot p_1 g^\mu_\sigma)}{(p_2-k)^2}\\ &-\frac{(g^{\mu\nu}(p_1-p_2)^\sigma + g^{\nu\sigma}(p_1+2p_2)^\mu - g^{\mu\sigma}(2p_1+p_2)^\nu)((p_1+p_2)^\rho k_\sigma - k\cdot(p_1+p_2)g^\rho_\sigma)}{(p_1+p_2)^2}\\ &+g^{\mu\nu}(p_1-p_2)^\rho + g^{\nu\rho}(p_2+k)^\mu - g^{\mu\rho}(k+p_1)^\nu\Bigg]\,,\end{aligned} \tag{A.10}$$



JCAP06(2014)060

$$\mathcal{M}_{D13} = -\frac{g_s^3}{4\pi}\frac{1}{\Lambda^3} f_{abc}\epsilon_\mu(p_1)\epsilon_\nu(p_2)\epsilon^*_\rho(k)\bar{u}(p_3)v(p_4)$$
$$\Bigg[\frac{(g^\mu_\sigma(2p_1-k)^\rho + g^\rho_\sigma(2k-p_1)^\mu - g^{\mu\rho}(k+p_1)_\sigma)(\epsilon^{\sigma\nu\eta\chi}p_{2\eta}(p_1-k)_\chi))}{(p_1-k)^2}$$
$$+\frac{(g^\nu_\sigma(2p_2-k)^\rho + g^\rho_\sigma(2k-p_2)^\nu - g^{\nu\rho}(k+p_2)_\sigma)(\epsilon^{\sigma\mu\eta\chi}p_{1\eta}(p_2-k)_\chi)}{(p_2-k)^2}$$
$$+\frac{(g^{\mu\nu}(p_1-p_2)_\sigma + g^\nu_\sigma(p_1+2p_2)^\mu - g^\mu_\sigma(2p_1+p_2)^\nu)(\epsilon^{\rho\eta\sigma\chi}k_\eta(p_1+p_2)_\chi)}{(p_1+p_2)^2}$$
$$-\epsilon^{\mu\nu\rho\sigma}(p_1+p_2-k)_\sigma\Bigg], \tag{A.11}$$

$$\mathcal{M}_{D14} = -i\frac{g_s^3}{4\pi}\frac{1}{\Lambda^3} f_{abc}\epsilon_\mu(p_1)\epsilon_\nu(p_2)\epsilon^*_\rho(k)\bar{u}(p_3)\gamma^5 v(p_4)$$
$$\Bigg[\frac{(g^\mu_\sigma(2p_1-k)^\rho + g^\rho_\sigma(2k-p_1)^\mu - g^{\mu\rho}(k+p_1)_\sigma)(\epsilon^{\sigma\nu\eta\chi}p_{2\eta}(p_1-k)_\chi))}{(p_1-k)^2}$$
$$+\frac{(g^\nu_\sigma(2p_2-k)^\rho + g^\rho_\sigma(2k-p_2)^\nu - g^{\nu\rho}(k+p_2)_\sigma)(\epsilon^{\sigma\mu\eta\chi}p_{1\eta}(p_2-k)_\chi)}{(p_2-k)^2}$$
$$+\frac{(g^{\mu\nu}(p_1-p_2)_\sigma + g^\nu_\sigma(p_1+2p_2)^\mu - g^\mu_\sigma(2p_1+p_2)^\nu)(\epsilon^{\rho\eta\sigma\chi}k_\eta(p_1+p_2)_\chi)}{(p_1+p_2)^2}$$
$$-\epsilon^{\mu\nu\rho\sigma}(p_1+p_2-k)_\sigma\Bigg]. \tag{A.12}$$

where $p_1, p_2$ are the initial momenta, $k$ the momenta of the gluon, and $p_3, p_4$ the momenta of the DM particle/antiparticle, $g_s$ is the SU(3) gauge coupling and $T^a$ are the SU(3) generators in the fundamental representation.

The corresponding squared amplitudes, averaged over initial states (color and spin) and summed over the final states are

$$\sum\overline{|\mathcal{M}_{D1'}|^2} = \frac{16}{9}\frac{g_s^2}{\Lambda^4}\frac{[(p_3\cdot p_4)-m^2_{\rm DM}]\left[(k\cdot(p_1+p_2))^2 - 2(p_1\cdot p_2)(k\cdot p_1 + k\cdot p_2 - p_1\cdot p_2)\right]}{(k\cdot p_1)(k\cdot p_2)}, \tag{A.13}$$

$$\sum\overline{|\mathcal{M}_{D4'}|^2} = \frac{16}{9}\frac{g_s^2}{\Lambda^4}\frac{[(p_3\cdot p_4)+m^2_{\rm DM}]\left[(k\cdot(p_1+p_2))^2 - 2(p_1\cdot p_2)(k\cdot p_1 + k\cdot p_2 - p_1\cdot p_2)\right]}{(k\cdot p_1)(k\cdot p_2)}, \tag{A.14}$$

$$\sum\overline{|\mathcal{M}_{D5}|^2} = -\frac{32}{9}\frac{g_s^2}{\Lambda^4}\Bigg[\frac{(k\cdot p_1)\left[(k\cdot p_1)+(k\cdot p_2)-3(p_1\cdot p_2)-m^2_{\rm DM}\right]}{(k\cdot p_2)}$$
$$+\frac{(k\cdot p_2)\left[(k\cdot p_1)+(k\cdot p_2)-3(p_1\cdot p_2)-m^2_{\rm DM}\right]}{(k\cdot p_1)} - 4(p_1\cdot p_2)$$
$$-2\frac{(p_1\cdot p_2)}{(k\cdot p_1)(k\cdot p_2)}\left[(k\cdot p_3)\left((p_1\cdot p_3)+(p_2\cdot p_3)\right) + (p_1\cdot p_2)\left(m^2_{\rm DM}+(p_1\cdot p_2)\right)\right.$$
$$\left.-2(p_1\cdot p_3)(p_2\cdot p_3)\right]$$
$$+2\frac{(k\cdot p_3)(p_1\cdot p_3) - (p_2\cdot p_3)(p_1\cdot p_3) + (p_2\cdot p_3)^2 + 2(p_1\cdot p_2)^2 + m^2_{\rm DM}(p_1\cdot p_2)}{(k\cdot p_2)}$$
$$+2\frac{(k\cdot p_3)(p_2\cdot p_3) - (p_1\cdot p_3)(p_2\cdot p_3) + (p_1\cdot p_3)^2 + 2(p_1\cdot p_2)^2 + m^2_{\rm DM}(p_1\cdot p_2)}{(k\cdot p_1)}\Bigg], \tag{A.15}$$

$$\sum\overline{|\mathcal{M}_{D8}|^2} = \frac{32}{9}\frac{g_s^2}{\Lambda^4}\Bigg[\frac{(k\cdot p_1)\left[(k\cdot p_1)+(k\cdot p_2)-3(p_1\cdot p_2)+m^2_{\rm DM}+2(p_3\cdot p_4)\right]}{(k\cdot p_2)}$$
$$+\frac{(k\cdot p_2)\left[(k\cdot p_1)+(k\cdot p_2)-3(p_1\cdot p_2)+m^2_{\rm DM}+2(p_3\cdot p_4)\right]}{(k\cdot p_1)} - 4(p_1\cdot p_2)$$



JCAP06(2014)060

$$
\begin{aligned}
&+2\frac{(p_1\cdot p_2)}{(k\cdot p_1)(k\cdot p_2)}\left[(p_1\cdot p_2)\left(2(p_3\cdot p_4)+m_{\rm DM}^2\right)+(k\cdot p_3)\left((p_1\cdot p_3)+(p_2\cdot p_3)\right)\right.\\
&\left.+2(p_1\cdot p_3)(p_2\cdot p_3)-(p_1\cdot p_2)^2\right]\\
&+2\frac{(p_1\cdot p_3)\left[-(k\cdot p_3)+(p_2\cdot p_3)\right]-(p_2\cdot p_3)^2+(p_1\cdot p_2)\left[2(p_1\cdot p_2)-m_{\rm DM}^2-2(p_3\cdot p_4)\right]}{(k\cdot p_2)}\\
&\left.+2\frac{(p_2\cdot p_3)\left[-(k\cdot p_3)+(p_1\cdot p_3)\right]-(p_1\cdot p_3)^2+(p_1\cdot p_2)\left[2(p_1\cdot p_2)-m_{\rm DM}^2-2(p_3\cdot p_4)\right]}{(k\cdot p_1)}\right],
\end{aligned}
\tag{A.16}
$$

$$
\begin{aligned}
\sum\overline{|\mathcal{M}_{D9}|^2} = \frac{128}{9}\frac{g_s^2}{\Lambda^4}\Bigg[&-2[m_{\rm DM}^2-(k\cdot p_3)]+\frac{(k\cdot p_1)\left[-(k\cdot p_3)+(p_1\cdot p_3)-(p_2\cdot p_3)+m_{\rm DM}^2\right]}{(k\cdot p_2)}\\
&-2\frac{(p_1\cdot p_2)\left[-2(k\cdot p_3)+(p_1\cdot p_3)+(p_2\cdot p_3)+m_{\rm DM}^2\right]}{(k\cdot p_2)}\\
&-4\frac{\left[(k\cdot p_3)-(p_2\cdot p_3)\right]\left[(p_1\cdot p_3)-(p_2\cdot p_3)\right]}{(k\cdot p_2)}\\
&+\frac{(k\cdot p_2)\left[-(k\cdot p_3)+(p_2\cdot p_3)-(p_1\cdot p_3)+m_{\rm DM}^2\right]}{(k\cdot p_1)}\\
&-2\frac{(p_1\cdot p_2)\left[-2(k\cdot p_3)+(p_1\cdot p_3)+(p_2\cdot p_3)+m_{\rm DM}^2\right]}{(k\cdot p_1)}\\
&-4\frac{\left[(k\cdot p_3)-(p_1\cdot p_3)\right]\left[(p_2\cdot p_3)-(p_1\cdot p_3)\right]}{(k\cdot p_1)}\\
&-2\frac{(p_1\cdot p_2)\left[(k\cdot p_3)-(p_1\cdot p_3)-(p_2\cdot p_3)\right]\left[2(k\cdot p_3)+(p_1\cdot p_2)\right]}{(k\cdot p_1)(k\cdot p_2)}\\
&+2\frac{(p_1\cdot p_2)\left[-4(p_1\cdot p_3)(p_2\cdot p_3)+m_{\rm DM}^2(p_1\cdot p_2)\right]}{(k\cdot p_1)(k\cdot p_2)}\Bigg],
\end{aligned}
\tag{A.17}
$$

$$
\begin{aligned}
\sum\overline{|\mathcal{M}_{D11}|^2} = \frac{3}{32\pi^2}\frac{g_s^6}{\Lambda^6}\left[(p_3\cdot p_4)-m_{\rm DM}^2\right]\Bigg\{&\frac{(k\cdot p_1)^3}{(k\cdot p_2)(p_1\cdot p_2)}+\frac{(k\cdot p_2)^3}{(k\cdot p_1)(p_1\cdot p_2)}+\frac{(p_1\cdot p_2)^3}{(k\cdot p_1)(k\cdot p_2)}\\
&+3\frac{(k\cdot p_1)(k\cdot p_2)}{(p_1\cdot p_2)}+\frac{(k\cdot p_1)(p_1\cdot p_2)-(k\cdot p_1)^2}{(k\cdot p_2)}+\frac{(k\cdot p_2)(p_1\cdot p_2)-(k\cdot p_2)^2}{(k\cdot p_1)}\\
&-\frac{(k_-\cdot p_1)(k\cdot p_2)^3}{(k\cdot k_-)(k\cdot p_1)(p_1\cdot p_2)}-\frac{(k_-\cdot p_2)(k\cdot p_1)^3}{(k\cdot k_-)(k\cdot p_2)(p_1\cdot p_2)}\\
&+\frac{(k_-\cdot p_1)}{(k\cdot k_-)(p_1\cdot p_2)}[(k\cdot p_1)^2+(k\cdot p_1)(k\cdot p_2)-(k\cdot p_2)^2]\\
&+\frac{(k_-\cdot p_2)}{(k\cdot k_-)(p_1\cdot p_2)}[(k\cdot p_2)^2+(k\cdot p_1)(k\cdot p_2)-(k\cdot p_1)^2]\\
&+2\frac{(k_-\cdot p_1)}{(k\cdot k_-)(k\cdot p_1)}[(k\cdot p_2)^2-(p_1\cdot p_2)(k\cdot p_2)]\\
&+2\frac{(k_-\cdot p_2)}{(k\cdot k_-)(k\cdot p_2)}[(k\cdot p_1)^2-(p_1\cdot p_2)(k\cdot p_1)]\\
&+2\frac{(k_-\cdot p_1)}{(k\cdot k_-)}[(p_1\cdot p_2)+(k\cdot p_1)-2(k\cdot p_2)]\\
&+2\frac{(k_-\cdot p_2)}{(k\cdot k_-)}[(p_1\cdot p_2)+(k\cdot p_2)-2(k\cdot p_1)]\\
&+(k\cdot p_1)+(k\cdot p_2)+6(p_1\cdot p_2)\Bigg\},
\end{aligned}
\tag{A.18}
$$



JCAP06(2014)060

$$
\begin{aligned}
\sum \overline{|\mathcal{M}_{D12}|^2} = \frac{3}{32\pi^2}\frac{g_s^6}{\Lambda^6}\left[(p_3\cdot p_4)+m_{\rm DM}^2\right]\Bigg\{&\frac{(k\cdot p_1)^3}{(k\cdot p_2)(p_1\cdot p_2)}+\frac{(k\cdot p_2)^3}{(k\cdot p_1)(p_1\cdot p_2)}+\frac{(p_1\cdot p_2)^3}{(k\cdot p_1)(k\cdot p_2)}\\
&+3\frac{(k\cdot p_1)(k\cdot p_2)}{(p_1\cdot p_2)}+\frac{(k\cdot p_1)(p_1\cdot p_2)-(k\cdot p_1)^2}{(k\cdot p_2)}+\frac{(k\cdot p_2)(p_1\cdot p_2)-(k\cdot p_2)^2}{(k\cdot p_1)}\\
&-\frac{(k_-\cdot p_1)(k\cdot p_2)^3}{(k\cdot k_-)(k\cdot p_1)(p_1\cdot p_2)}-\frac{(k_-\cdot p_2)(k\cdot p_1)^3}{(k\cdot k_-)(k\cdot p_2)(p_1\cdot p_2)}\\
&+\frac{(k_-\cdot p_1)}{(k\cdot k_-)(p_1\cdot p_2)}[(k\cdot p_1)^2+(k\cdot p_1)(k\cdot p_2)-(k\cdot p_2)^2]\\
&+\frac{(k_-\cdot p_2)}{(k\cdot k_-)(p_1\cdot p_2)}[(k\cdot p_2)^2+(k\cdot p_1)(k\cdot p_2)-(k\cdot p_1)^2]\\
&+2\frac{(k_-\cdot p_1)}{(k\cdot k_-)(k\cdot p_1)}[(k\cdot p_2)^2-(p_1\cdot p_2)(k\cdot p_2)]\\
&+2\frac{(k_-\cdot p_2)}{(k\cdot k_-)(k\cdot p_2)}[(k\cdot p_1)^2-(p_1\cdot p_2)(k\cdot p_1)]\\
&+2\frac{(k_-\cdot p_1)}{(k\cdot k_-)}[(p_1\cdot p_2)+(k\cdot p_1)-2(k\cdot p_2)]\\
&+2\frac{(k_-\cdot p_2)}{(k\cdot k_-)}[(p_1\cdot p_2)+(k\cdot p_2)-2(k\cdot p_1)]\\
&+(k\cdot p_1)+(k\cdot p_2)+6(p_1\cdot p_2)\Bigg\},
\end{aligned}
\tag{A.19}
$$

$$
\begin{aligned}
\sum \overline{|\mathcal{M}_{D13}|^2} = \frac{3}{32\pi^2}\frac{g_s^6}{\Lambda^6}\left[(p_3\cdot p_4)-m_{\rm DM}^2\right]\Bigg\{&\frac{(k\cdot p_1)^3}{(k\cdot p_2)(p_1\cdot p_2)}+\frac{(k\cdot p_2)^3}{(k\cdot p_1)(p_1\cdot p_2)}+\frac{(p_1\cdot p_2)^3}{(k\cdot p_1)(k\cdot p_2)}\\
&+3\frac{(k\cdot p_1)(k\cdot p_2)}{(p_1\cdot p_2)}+\frac{(k\cdot p_1)(p_1\cdot p_2)-(k\cdot p_1)^2}{(k\cdot p_2)}+\frac{(k\cdot p_2)(p_1\cdot p_2)-(k\cdot p_2)^2}{(k\cdot p_1)}\\
&-\frac{(k_-\cdot p_1)(k\cdot p_2)^3}{(k\cdot k_-)(k\cdot p_1)(p_1\cdot p_2)}-\frac{(k_-\cdot p_2)(k\cdot p_1)^3}{(k\cdot k_-)(k\cdot p_2)(p_1\cdot p_2)}\\
&+\frac{(k_-\cdot p_1)}{(k\cdot k_-)(p_1\cdot p_2)}[(k\cdot p_1)^2-3(k\cdot p_1)(k\cdot p_2)+3(k\cdot p_2)^2]\\
&+\frac{(k_-\cdot p_2)}{(k\cdot k_-)(p_1\cdot p_2)}[(k\cdot p_2)^2-3(k\cdot p_1)(k\cdot p_2)+3(k\cdot p_1)^2]\\
&+2\frac{(k_-\cdot p_1)}{(k\cdot k_-)(k\cdot p_1)}[(k\cdot p_2)^2-(p_1\cdot p_2)(k\cdot p_2)]\\
&+2\frac{(k_-\cdot p_2)}{(k\cdot k_-)(k\cdot p_2)}[(k\cdot p_1)^2-(p_1\cdot p_2)(k\cdot p_1)]\\
&+2\frac{(k_-\cdot p_1)}{(k\cdot k_-)}[(p_1\cdot p_2)+(k\cdot p_1)-2(k\cdot p_2)]\\
&+2\frac{(k_-\cdot p_2)}{(k\cdot k_-)}[(p_1\cdot p_2)+(k\cdot p_2)-2(k\cdot p_1)]\\
&-3(k\cdot p_1)-3(k\cdot p_2)+2(p_1\cdot p_2)\Bigg\},
\end{aligned}
\tag{A.20}
$$

$$
\begin{aligned}
\sum \overline{|\mathcal{M}_{D14}|^2} = \frac{3}{32\pi^2}\frac{g_s^6}{\Lambda^6}\left[(p_3\cdot p_4)+m_{\rm DM}^2\right]\Bigg\{&\frac{(k\cdot p_1)^3}{(k\cdot p_2)(p_1\cdot p_2)}+\frac{(k\cdot p_2)^3}{(k\cdot p_1)(p_1\cdot p_2)}+\frac{(p_1\cdot p_2)^3}{(k\cdot p_1)(k\cdot p_2)}\\
&+3\frac{(k\cdot p_1)(k\cdot p_2)}{(p_1\cdot p_2)}+\frac{(k\cdot p_1)(p_1\cdot p_2)-(k\cdot p_1)^2}{(k\cdot p_2)}+\frac{(k\cdot p_2)(p_1\cdot p_2)-(k\cdot p_2)^2}{(k\cdot p_1)}\\
&-\frac{(k_-\cdot p_1)(k\cdot p_2)^3}{(k\cdot k_-)(k\cdot p_1)(p_1\cdot p_2)}-\frac{(k_-\cdot p_2)(k\cdot p_1)^3}{(k\cdot k_-)(k\cdot p_2)(p_1\cdot p_2)}
\end{aligned}
$$



JCAP06(2014)060

$$
\begin{aligned}
&+\frac{(k_-\cdot p_1)}{(k\cdot k_-)(p_1\cdot p_2)}[(k\cdot p_1)^2-3(k\cdot p_1)(k\cdot p_2)+3(k\cdot p_2)^2]\\
&+\frac{(k_-\cdot p_2)}{(k\cdot k_-)(p_1\cdot p_2)}[(k\cdot p_2)^2-3(k\cdot p_1)(k\cdot p_2)+3(k\cdot p_1)^2]\\
&+2\frac{(k_-\cdot p_1)}{(k\cdot k_-)(k\cdot p_1)}[(k\cdot p_2)^2-(p_1\cdot p_2)(k\cdot p_2)]\\
&+2\frac{(k_-\cdot p_2)}{(k\cdot k_-)(k\cdot p_2)}[(k\cdot p_1)^2-(p_1\cdot p_2)(k\cdot p_1)]\\
&+2\frac{(k_-\cdot p_1)}{(k\cdot k_-)}[(p_1\cdot p_2)+(k\cdot p_1)-2(k\cdot p_2)]+2\frac{(k_-\cdot p_2)}{(k\cdot k_-)}[(p_1\cdot p_2)+(k\cdot p_2)-2(k\cdot p_1)]\\
&-3(k\cdot p_1)-3(k\cdot p_2)+2(p_1\cdot p_2)\Big\}\,. \qquad \text{(A.21)}
\end{aligned}
$$

where the polarization 4-vector is defined as $k_-\equiv P(k^\nu)/\sqrt{k^\mu\cdot P(k_\mu)}$, where $P$ is the parity operation.

### A.3 Cross sections

Now, the next step is to compute the cross sections in the lab frame. To this end we proceed by first evaluating the matrix elements and the phase space density in the center-of-mass frame and then boosting the result to the lab frame. In the center-of-mass (c.o.m) frame, let us parametrize the four-momenta inolved in the process as

$$
\begin{aligned}
&p_1=x\frac{\sqrt{s}}{2}(1,0,0,1)\,,\qquad p_2=x\frac{\sqrt{s}}{2}(1,0,0,-1)\,,\qquad k=x\frac{\sqrt{s}}{2}(z_0,z_0\hat{k})\,, \qquad \text{(A.22)}\\
&p_3=x\frac{\sqrt{s}}{2}(1-y_0,\sqrt{(1-y_0)^2-a^2}\hat{p}_3)\,,\quad p_4=x\frac{\sqrt{s}}{2}(1+y_0-z_0,\sqrt{(1+y_0-z_0)^2-a^2}\hat{p}_4)\,,
\end{aligned}
$$

where the two colliding partons carry equal momentum fractions $x_1=x_2\equiv x$ of the incoming protons, $a\equiv 2m_{\rm DM}/(x\sqrt{s})<1$, $\hat{k}=(0,\sin\theta_0,\cos\theta_0)$, and $\theta_0$ is the polar angle of $\hat{k}$ with respect to the beam line, in the c.o.m. frame. With the subscript $_0$ we will refer to quantities evaluated in the c.o.m. frame. The polarization 4-vector $k_-$ in the c.o.m. frame simply reads $k_-=(1/\sqrt{2})(1,0,-\sin\theta_0,-\cos\theta_0)$.

The conservation of three-momentum sets the angle $\theta_{0\,3j}$ between $\hat{p}_3$ and $\hat{k}$ as: $\cos\theta_{0\,3j}=(\mathbf{p}_4^2-\mathbf{k}^2-\mathbf{p}_3^2)/2|\mathbf{k}||\mathbf{p}_3|$. For the doubly-differential cross sections with respect to the energy and angle of the emitted gluon, in the c.o.m. frame, we obtain

$$
\begin{aligned}
\left.\frac{{\rm d}^2\hat{\sigma}}{{\rm d}z_0{\rm d}\cos\theta_0}\right|_{D1'} &= \frac{\alpha_s}{36\pi^2}\frac{x^2s}{\Lambda^4}\frac{\left[1-z_0-\frac{4m_{\rm DM}^2}{x^2s}\right]^{3/2}}{\sqrt{1-z_0}}\frac{[1+(1-z_0)^2]}{z_0\sin^2\theta_0}\,, &\text{(A.23)}\\
\left.\frac{{\rm d}^2\hat{\sigma}}{{\rm d}z_0{\rm d}\cos\theta_0}\right|_{D4'} &= \frac{\alpha_s}{36\pi^2}\frac{x^2s}{\Lambda^4}\frac{\left[1-z_0-\frac{4m_{\rm DM}^2}{x^2s}\right]^{1/2}}{\sqrt{1-z_0}}\frac{[1+(1-z_0)^2]}{z_0\sin^2\theta_0}\,, &\text{(A.24)}\\
\left.\frac{{\rm d}^2\hat{\sigma}}{{\rm d}z_0{\rm d}\cos\theta_0}\right|_{D5} &= \frac{\alpha_s}{108\pi^2}\frac{x^2s}{\Lambda^4}\frac{\sqrt{1-z_0-\frac{4m_{\rm DM}^2}{x^2s}}}{\sqrt{1-z_0}}\frac{\left(1-z_0+\frac{2m_{\rm DM}^2}{x^2s}\right)(8-8z_0+(3+\cos2\theta_0)z_0^2)}{z_0\sin^2\theta_0}\,, &\text{(A.25)}\\
\left.\frac{{\rm d}^2\hat{\sigma}}{{\rm d}z_0{\rm d}\cos\theta_0}\right|_{D8} &= \frac{\alpha_s}{108\pi^2}\frac{x^2s}{\Lambda^4}\frac{[1-z_0-\frac{4m_{\rm DM}^2}{x^2s}]^{3/2}}{\sqrt{1-z_0}}\frac{8-8z_0+(3+\cos2\theta_0)z_0^2}{z_0\sin^2\theta_0}\,, &\text{(A.26)}\\
\left.\frac{{\rm d}^2\hat{\sigma}}{{\rm d}z_0{\rm d}\cos\theta_0}\right|_{D9} &= \frac{\alpha_s}{27\pi^2}\frac{x^2s}{\Lambda^4}\frac{\sqrt{1-z_0-\frac{4m_{\rm DM}^2}{x^2s}}}{[1-z_0]^{3/2}}\frac{\left(1-z_0+\frac{2m_{\rm DM}^2}{x^2s}\right)(4-8z_0+6z_0^2-(1+\cos2\theta_0)z_0^3)}{z_0\sin^2\theta_0}\,,
\end{aligned}
$$



JCAP06(2014)060

(A.27)

$$\left.\frac{\mathrm{d}^2\hat{\sigma}}{\mathrm{d}z_0\mathrm{d}\cos\theta_0}\right|_{D11} = \frac{3\alpha_s^3 x^4 s^2}{32768\pi^2\Lambda^6}\frac{\left[1-z_0-\frac{4m_{\rm DM}^2}{x^2 s}\right]^{3/2}}{z_0\sqrt{1-z_0}\sin^2\theta_0}\left[128-128(1+\cos 2\theta_0)z_0\right.$$
$$+(304+64\cos 2\theta_0+16\cos 4\theta_0)z_0^2-128(1+\cos 2\theta_0)z_0^3$$
$$\left.+(79+44\cos 2\theta_0+5\cos 4\theta_0)z_0^4\right]\,, \tag{A.28}$$

$$\left.\frac{\mathrm{d}^2\hat{\sigma}}{\mathrm{d}z_0\mathrm{d}\cos\theta_0}\right|_{D12} = \frac{3\alpha_s^3 x^4 s^2}{32768\pi^2\Lambda^6}\frac{\sqrt{1-z_0-\frac{4m_{\rm DM}^2}{x^2 s}}\sqrt{1-z_0}}{z_0\sin^2\theta_0}\left[128-128(1+\cos 2\theta_0)z_0\right.$$
$$+(304+64\cos 2\theta_0+16\cos 4\theta_0)z_0^2-128(1+\cos 2\theta_0)z_0^3$$
$$\left.+(79+44\cos 2\theta_0+5\cos 4\theta_0)z_0^4\right]\,, \tag{A.29}$$

$$\left.\frac{\mathrm{d}^2\hat{\sigma}}{\mathrm{d}z_0\mathrm{d}\cos\theta_0}\right|_{D13} = \frac{3\alpha_s^3 x^4 s^2}{32768\pi^2\Lambda^6}\frac{\left[1-z_0-\frac{4m_{\rm DM}^2}{x^2 s}\right]^{3/2}}{z_0\sqrt{1-z_0}\sin^2\theta_0}\left[128-128(1+\cos 2\theta_0)z_0\right.$$
$$+(240+128\cos 2\theta_0+16\cos 4\theta_0)z_0^2-16(11+4\cos 2\theta_0+\cos 4\theta_0)z_0^3$$
$$\left.+(79+44\cos 2\theta_0+5\cos 4\theta_0)z_0^4\right]\,, \tag{A.30}$$

$$\left.\frac{\mathrm{d}^2\hat{\sigma}}{\mathrm{d}z_0\mathrm{d}\cos\theta_0}\right|_{D14} = \frac{3\alpha_s^3 x^4 s^2}{32768\pi^2\Lambda^6}\frac{\sqrt{1-z_0-\frac{4m_{\rm DM}^2}{x^2 s}}\sqrt{1-z_0}}{z_0\sin^2\theta_0}\left[128-128(1+\cos 2\theta_0)z_0\right.$$
$$+(240+128\cos 2\theta_0+16\cos 4\theta_0)z_0^2-16(11+4\cos 2\theta_0+\cos 4\theta_0)z_0^3$$
$$\left.+(79+44\cos 2\theta_0+5\cos 4\theta_0)z_0^4\right]\,. \tag{A.31}$$

Eq. (A.23)–(A.26) agree with the findings in refs. [24, 25], up to the factor of 1/9, as we are considering colored colliding particles.

To get the cross sections in the lab frame we perform a boost along the $\hat{z}$-axis, accounting for generic parton momentum fractions $x_1, x_2$. Also, the energy and angle of the emitted gluon are translated into momentum transfer $p_{\rm T}$ and pseudo-rapidity $\eta$. This way we get the translation of eqs. (A.23)–(A.27) into the lab frame

$$\left.\frac{\mathrm{d}^2\hat{\sigma}}{\mathrm{d}p_{\rm T}\mathrm{d}\eta}\right|_{D1'} = \frac{\alpha_s}{36\pi^2}\frac{x_1x_2s}{\Lambda^4}\frac{1}{p_{\rm T}}\frac{\left[1-f-\frac{4m_{\rm DM}^2}{x_1x_2s}\right]^{3/2}\left[1+(1-f)^2\right]}{\sqrt{1-f}}\,, \tag{A.32}$$

$$\left.\frac{\mathrm{d}^2\hat{\sigma}}{\mathrm{d}p_{\rm T}\mathrm{d}\eta}\right|_{D4'} = \frac{\alpha_s}{36\pi^2}\frac{x_1x_2s}{\Lambda^4}\frac{\sqrt{1-f}}{p_{\rm T}}\left[1-f-\frac{4m_{\rm DM}^2}{x_1x_2s}\right]^{1/2}\left[1+(1-f)^2\right]\,, \tag{A.33}$$

$$\left.\frac{\mathrm{d}^2\hat{\sigma}}{\mathrm{d}p_{\rm T}\mathrm{d}\eta}\right|_{D5} = \frac{\alpha_s}{27\pi^2}\frac{x_1x_2s}{\Lambda^4}\frac{\sqrt{1-f-\frac{4m_{\rm DM}^2}{x_1x_2s}}}{\sqrt{1-f}}\frac{\left[1-f+\frac{2m_{\rm DM}^2}{x_1x_2s}\right]\left[1+(1-f)^2-2\frac{p_{\rm T}^2}{x_1x_2s}\right]}{p_{\rm T}}\,, \tag{A.34}$$

$$\left.\frac{\mathrm{d}^2\hat{\sigma}}{\mathrm{d}p_{\rm T}\mathrm{d}\eta}\right|_{D8} = \frac{\alpha_s}{27\pi^2}\frac{x_1x_2s}{\Lambda^4}\frac{[1-f-\frac{4m_{\rm DM}^2}{x_1x_2s}]^{3/2}}{\sqrt{1-f}}\frac{1+(1-f)^2-2\frac{p_{\rm T}^2}{x_1x_2s}}{p_{\rm T}}\,, \tag{A.35}$$

$$\left.\frac{\mathrm{d}^2\hat{\sigma}}{\mathrm{d}p_{\rm T}\mathrm{d}\eta}\right|_{D9} = \frac{2\alpha_s}{27\pi^2}\frac{x_1x_2s}{\Lambda^4}\frac{\sqrt{1-f-\frac{4m_{\rm DM}^2}{sx_1x_2}}}{[1-f]^{3/2}}\frac{\left(1-f+\frac{2m_{\rm DM}^2}{x_1x_2s}\right)\left[(1-f)(1+(1-f)^2)+f\frac{4p_{\rm T}^2}{x_1x_2s}\right]}{p_{\rm T}}\,, \tag{A.36}$$

$$\left.\frac{\mathrm{d}^2\hat{\sigma}}{\mathrm{d}p_{\rm T}\mathrm{d}\eta}\right|_{D11} = \frac{3\alpha_s^3 x_1^2x_2^2s^2}{256\pi^2\Lambda^6}\frac{\left(1-f-\frac{4m_{\rm DM}^2}{sx_1x_2}\right)^{3/2}}{p_{\rm T}f^2\sqrt{1-f}}\left[16\frac{p_{\rm T}^4}{x_1^2x_2^2s^2}+8\frac{p_{\rm T}^2}{x_1x_2s}f+\left(1-8\frac{p_{\rm T}^2}{x_1x_2s}+5\frac{p_{\rm T}^4}{x_1^2x_2^2s^2}\right)f^2\right.$$
$$\left.+\left(-2+8\frac{p_{\rm T}^2}{x_1x_2s}\right)f^3+\left(3-4\frac{p_{\rm T}^2}{x_1x_2s}\right)f^4-2f^5+f^6\right]\,, \tag{A.37}$$



JCAP06(2014)060

$$\left.\frac{\mathrm{d}^2\hat{\sigma}}{\mathrm{d}p_{\mathrm{T}}\mathrm{d}\eta}\right|_{D12} = \frac{3\alpha_s^3 x_1^2 x_2^2 s^2}{256\pi^2\Lambda^6}\frac{\sqrt{1-f-\frac{4m_{\mathrm{DM}}^2}{sx_1x_2}}\sqrt{1-f}}{p_{\mathrm{T}}f^2}\left[16\frac{p_{\mathrm{T}}^4}{x_1^2x_2^2s^2}+8\frac{p_{\mathrm{T}}^2}{x_1x_2s}f\right.$$
$$+\left(1-8\frac{p_{\mathrm{T}}^2}{x_1x_2s}+5\frac{p_{\mathrm{T}}^4}{x_1^2x_2^2s^2}\right)f^2+\left(-2+8\frac{p_{\mathrm{T}}^2}{x_1x_2s}\right)f^3$$
$$\left.+\left(3-4\frac{p_{\mathrm{T}}^2}{x_1x_2s}\right)f^4-2f^5+f^6\right], \tag{A.38}$$

$$\left.\frac{\mathrm{d}^2\hat{\sigma}}{\mathrm{d}p_{\mathrm{T}}\mathrm{d}\eta}\right|_{D13} = \frac{3\alpha_s^3 x_1^2 x_2^2 s^2}{256\pi^2\Lambda^6}\frac{\left(1-f-\frac{4m_{\mathrm{DM}}^2}{sx_1x_2}\right)^{3/2}}{p_{\mathrm{T}}f^2\sqrt{1-f}}\left[16\frac{p_{\mathrm{T}}^4}{x_1^2x_2^2s^2}+8\left(\frac{p_{\mathrm{T}}^2}{x_1x_2s}-2\frac{p_{\mathrm{T}}^4}{x_1^2x_2^2s^2}\right)f\right.$$
$$+\left(1-12\frac{p_{\mathrm{T}}^2}{x_1x_2s}+5\frac{p_{\mathrm{T}}^4}{x_1^2x_2^2s^2}\right)f^2+\left(-2+8\frac{p_{\mathrm{T}}^2}{x_1x_2s}\right)f^3$$
$$\left.+\left(3-4\frac{p_{\mathrm{T}}^2}{x_1x_2s}\right)f^4-2f^5+f^6\right], \tag{A.39}$$

$$\left.\frac{\mathrm{d}^2\hat{\sigma}}{\mathrm{d}p_{\mathrm{T}}\mathrm{d}\eta}\right|_{D14} = \frac{3\alpha_s^3 x_1^2 x_2^2 s^2}{256\pi^2\Lambda^6}\frac{\sqrt{1-f-\frac{4m_{\mathrm{DM}}^2}{sx_1x_2}}\sqrt{1-f}}{p_{\mathrm{T}}f^2}\left[16\frac{p_{\mathrm{T}}^4}{x_1^2x_2^2s^2}+8\left(\frac{p_{\mathrm{T}}^2}{x_1x_2s}-2\frac{p_{\mathrm{T}}^4}{x_1^2x_2^2s^2}\right)f\right.$$
$$+\left(1-12\frac{p_{\mathrm{T}}^2}{x_1x_2s}+5\frac{p_{\mathrm{T}}^4}{x_1^2x_2^2s^2}\right)f^2+\left(-2+8\frac{p_{\mathrm{T}}^2}{x_1x_2s}\right)f^3$$
$$\left.+\left(3-4\frac{p_{\mathrm{T}}^2}{x_1x_2s}\right)f^4-2f^5+f^6\right], \tag{A.40}$$

where we have defined

$$f(p_{\mathrm{T}},\eta,x_1,x_2) \equiv \frac{p_{\mathrm{T}}(x_1e^{-\eta}+x_2e^{\eta})}{x_1x_2\sqrt{s}}. \tag{A.41}$$

For the emission of a photon, rather than a gluon, from a quark with charge $Q_q$ one simply replaces $(4/3)\,\alpha_s \to Q_q^2\alpha$ in eqs. (A.32)–(A.36). From these expressions one reproduces the results reported in eqs. (2.5)–(2.13).

## References


[1] Planck collaboration, P.A.R. Ade et al., *Planck 2013 results. XVI. Cosmological parameters*, arXiv:1303.5076 [INSPIRE].

[2] M. Cirelli, *Indirect Searches for Dark Matter: a status review*, *Pramana* **79** (2012) 1021 [arXiv:1202.1454] [INSPIRE].

[3] L. Baudis, *Direct dark matter detection: the next decade*, *Phys. Dark Univ.* **1** (2012) 94 [arXiv:1211.7222] [INSPIRE].

[4] A. De Simone, V. Sanz and H.P. Sato, *Pseudo-Dirac Dark Matter Leaves a Trace*, *Phys. Rev. Lett.* **105** (2010) 121802 [arXiv:1004.1567] [INSPIRE].

[5] Y. Bai and A. Rajaraman, *Dark Matter Jets at the LHC*, arXiv:1109.6009 [INSPIRE].

[6] P.J. Fox, R. Harnik, R. Primulando and C.-T. Yu, *Taking a Razor to Dark Matter Parameter Space at the LHC*, *Phys. Rev.* **D 86** (2012) 015010 [arXiv:1203.1662] [INSPIRE].

[7] R.C. Cotta, J.L. Hewett, M.P. Le and T.G. Rizzo, *Bounds on Dark Matter Interactions with Electroweak Gauge Bosons*, *Phys. Rev.* **D 88** (2013) 116009 [arXiv:1210.0525] [INSPIRE].

[8] Y. Bai and T.M.P. Tait, *Searches with Mono-Leptons*, *Phys. Lett.* **B 723** (2013) 384 [arXiv:1208.4361] [INSPIRE].

[9] N.F. Bell, J.B. Dent, A.J. Galea, T.D. Jacques, L.M. Krauss et al., *Searching for Dark Matter at the LHC with a Mono-Z*, *Phys. Rev.* **D 86** (2012) 096011 [arXiv:1209.0231] [INSPIRE].




JCAP06(2014)060

[10] ATLAS collaboration, *Search for dark matter candidates and large extra dimensions in events with a jet and missing transverse momentum with the ATLAS detector*, *JHEP* **04** (2013) 075 [arXiv:1210.4491] [INSPIRE].

[11] CMS collaboration, *Search for New Physics with a Mono-Jet and Missing Transverse Energy in pp Collisions at* $\sqrt{s} = 7$ *TeV*, *Phys. Rev. Lett.* **107** (2011) 201804 [arXiv:1106.4775] [INSPIRE].

[12] ATLAS collaboration, *Search for New Phenomena in Monojet plus Missing Transverse Momentum Final States using* $10\,fb^{-1}$ *of pp Collisions at* $\sqrt{s} = 8$ *TeV with the ATLAS detector at the LHC*, ATLAS-CONF-2012-147 (2012).

[13] CMS collaboration, *Search for new physics in monojet events in pp collisions at* $\sqrt{s} = 8$ *TeV*, CMS-PAS-EXO-12-048 (2013).

[14] ATLAS collaboration, *Search for dark matter candidates and large extra dimensions in events with a photon and missing transverse momentum in pp collision data at* $\sqrt{s} = 7$ *TeV with the ATLAS detector*, *Phys. Rev. Lett.* **110** (2013) 011802 [arXiv:1209.4625] [INSPIRE].

[15] CMS collaboration, *Search for Dark Matter and Large Extra Dimensions in pp Collisions Yielding a Photon and Missing Transverse Energy*, *Phys. Rev. Lett.* **108** (2012) 261803 [arXiv:1204.0821] [INSPIRE].

[16] ATLAS collaboration, *Search for dark matter candidates and large extra dimensions in events with a photon and missing transverse momentum in pp collision data at* $\sqrt{s} = 7$ *TeV with the ATLAS detector*, ATLAS-CONF-2012-085 (2012).

[17] CMS collaboration, *Search for ADD Extra-dimensions in Monophotons*, CMS-PAS-EXO-11-058 (2011).

[18] M. Beltrán, D. Hooper, E.W. Kolb, Z.A.C. Krusberg and T.M.P. Tait, *Maverick dark matter at colliders*, *JHEP* **09** (2010) 037 [arXiv:1002.4137] [INSPIRE].

[19] J. Goodman, M. Ibe, A. Rajaraman, W. Shepherd, T.M.P. Tait et al., *Constraints on Light Majorana dark Matter from Colliders*, *Phys. Lett.* **B 695** (2011) 185 [arXiv:1005.1286] [INSPIRE].

[20] Y. Bai, P.J. Fox and R. Harnik, *The Tevatron at the Frontier of Dark Matter Direct Detection*, *JHEP* **12** (2010) 048 [arXiv:1005.3797] [INSPIRE].

[21] J. Goodman, M. Ibe, A. Rajaraman, W. Shepherd, T.M.P. Tait et al., *Constraints on Dark Matter from Colliders*, *Phys. Rev.* **D 82** (2010) 116010 [arXiv:1008.1783] [INSPIRE].

[22] A. Rajaraman, W. Shepherd, T.M.P. Tait and A.M. Wijangco, *LHC Bounds on Interactions of Dark Matter*, *Phys. Rev.* **D 84** (2011) 095013 [arXiv:1108.1196] [INSPIRE].

[23] P.J. Fox, R. Harnik, J. Kopp and Y. Tsai, *Missing Energy Signatures of Dark Matter at the LHC*, *Phys. Rev.* **D 85** (2012) 056011 [arXiv:1109.4398] [INSPIRE].

[24] H. Dreiner, M. Huck, M. Krämer, D. Schmeier and J. Tattersall, *Illuminating Dark Matter at the ILC*, *Phys. Rev.* **D 87** (2013) 075015 [arXiv:1211.2254] [INSPIRE].

[25] Y.J. Chae and M. Perelstein, *Dark Matter Search at a Linear Collider: Effective Operator Approach*, *JHEP* **05** (2013) 138 [arXiv:1211.4008] [INSPIRE].

[26] A. De Simone, A. Monin, A. Thamm and A. Urbano, *On the effective operators for Dark Matter annihilations*, *JCAP* **02** (2013) 039 [arXiv:1301.1486] [INSPIRE].

[27] H. Dreiner, D. Schmeier and J. Tattersall, *Contact Interactions Probe Effective Dark Matter Models at the LHC*, *Europhys. Lett.* **102** (2013) 51001 [arXiv:1303.3348] [INSPIRE].

[28] J.-Y. Chen, E.W. Kolb and L.-T. Wang, *Dark matter coupling to electroweak gauge and Higgs bosons: an effective field theory approach*, *Phys. Dark Univ.* **2** (2013) 200 [arXiv:1305.0021] [INSPIRE].

JCAP06(2014)060

[29] G. Busoni, A. De Simone, E. Morgante and A. Riotto, *On the Validity of the Effective Field Theory for Dark Matter Searches at the LHC*, *Phys. Lett.* **B 728** (2014) 412 [arXiv:1307.2253] [INSPIRE].

[30] O. Buchmueller, M.J. Dolan and C. McCabe, *Beyond Effective Field Theory for Dark Matter Searches at the LHC*, *JHEP* **01** (2014) 025 [arXiv:1308.6799] [INSPIRE].

[31] H. Dreiner, M. Huck, M. Krämer, D. Schmeier and J. Tattersall, *Illuminating Dark Matter at the ILC*, *Phys. Rev.* **D 87** (2013) 075015 [arXiv:1211.2254] [INSPIRE].

[32] P.J. Fox and C. Williams, *Next-to-Leading Order Predictions for Dark Matter Production at Hadron Colliders*, *Phys. Rev.* **D 87** (2013) 054030 [arXiv:1211.6390] [INSPIRE].

[33] H. An, X. Ji and L.-T. Wang, *Light Dark Matter and $Z'$ Dark Force at Colliders*, *JHEP* **07** (2012) 182 [arXiv:1202.2894] [INSPIRE].

[34] I.M. Shoemaker and L. Vecchi, *Unitarity and Monojet Bounds on Models for DAMA, CoGeNT and CRESST-II*, *Phys. Rev.* **D 86** (2012) 015023 [arXiv:1112.5457] [INSPIRE].

[35] P.J. Fox, R. Harnik, J. Kopp and Y. Tsai, *LEP Shines Light on Dark Matter*, *Phys. Rev.* **D 84** (2011) 014028 [arXiv:1103.0240] [INSPIRE].

[36] R. Barbieri, G. Isidori, J. Jones-Perez, P. Lodone and D.M. Straub, *U(2) and Minimal Flavour Violation in Supersymmetry*, *Eur. Phys. J.* **C 71** (2011) 1725 [arXiv:1105.2296] [INSPIRE].

[37] R. Barbieri, D. Buttazzo, F. Sala and D.M. Straub, *Flavour physics from an approximate $U(2)^3$ symmetry*, *JHEP* **07** (2012) 181 [arXiv:1203.4218] [INSPIRE].

[38] J. Alwall, M. Herquet, F. Maltoni, O. Mattelaer and T. Stelzer, *MadGraph 5 : Going Beyond*, *JHEP* **06** (2011) 128 [arXiv:1106.0522] [INSPIRE].

[39] A.D. Martin, W.J. Stirling, R.S. Thorne and G. Watt, *Parton distributions for the LHC*, *Eur. Phys. J.* **C 63** (2009) 189 [arXiv:0901.0002] [INSPIRE].

[40] S. Alekhin, S. Alioli, R.D. Ball, V. Bertone, J. Blumlein et al., *The PDF4LHC Working Group Interim Report*, arXiv:1101.0536 [INSPIRE].

[41] C. Doglioni and S. Schramm, private communication.

[42] G. Busoni, A. De Simone, T. Jacques, E. Morgante and A. Riotto, *On the Validity of the Effective Field Theory for Dark Matter Searches at the LHC Part III: Analysis for the t-channel*, arXiv:1405.3101 [INSPIRE].

JCAP06(2014)060